matoid arthritis[12, 13]; however, there has been much concern over the reactivation of viral infection caused by TNF blockade[14]. Shibata *et al.* compared the effects of PEG-R1antTNF and etanercept on antiviral immunity using a recombinant adenovirus vector and showed that PEG-R1antTNF did not reactivate viral infection, unlike etanercept[17]. Their results indicated that use of PEG-R1antTNF may reduce side effects such as increased susceptibility to viral infection due to its TNFR1 selectivity. Additionally, transmembrane TNF (tmTNF), the prime activating ligand of TNFR2[5], was reported to be sufficient to control Mycobacterium tuberculosis infection[37, 38], indicating the importance of TNF/TNFR2 function in this bacterial infection. Because PEG-R1antTNF does not bind TNFR2, PEG-R1antTNF cannot inhibit the interaction of tmTNF with TNFR2; therefore, we believe that PEG-R1antTNF would also have reduced side effects in the context of bacterial infection.

In conclusion, the present study shows that a selective TNFR1 antagonist, PEG-R1antTNF, suppresses arterial inflammation by inhibiting NF-κB activation and chemokine expression. Thus, inhibited TNFR1 signaling may provide a new therapeutic target for preventing intimal hyperplasia and inflammation.

Acknowledgements

We thank Mr. Shigehiro Kitada and Ms. Kozue Suzuki (Division of Basic Pathology, National Defense Medical College) for pathological support. We also thank the staff of the Institute of Laboratory Animals, National Defense Medical College for animal care.

Notice of Grant Support

This research was supported in part by National Defense Medical College Grant for Young Scientist (M.K.) and National Defense Medical College grant H14 (K.I.) and H18 (K.I.)

Disclosure

None.

References

1) Popa C, Netea MG, van Riel PL, van der Meer JW, Stalenhoef AF: The role of TNF-alpha in chronic inflammatory conditions, intermediary metabolism, and cardiovascular risk. J Lipid Res, 2007; 48: 751-762
2) Wajant H, Pfizenmaier K, Scheurich P: Tumor necrosis factor signaling. Cell Death Differ, 2003; 10: 45-65
3) Fan J, Watanabe T: Inflammatory reactions in the pathogenesis of atherosclerosis. J Atheroscler Thromb, 2003; 10: 63-71
4) Kleemann R, Zadelaar S, Kooistra T: Cytokines and atherosclerosis: a comprehensive review of studies in mice. Cardiovasc Res, 2008; 79: 360-376
5) Grell M, Douni E, Wajant H, Löhden M, Clauss M, Maxeiner B, Georgopoulos S, Lesslauer W, Kollias G, Pfizenmaier K, Scheurich P: The transmembrane form of tumor necrosis factor is the prime activating ligand of the 80 kDa tumor necrosis factor receptor. Cell, 1995; 83: 793-802
6) Schreyer SA, Peschon JJ, LeBoeuf RC: Accelerated atherosclerosis in mice lacking tumor necrosis factor receptor p55. J Biol Chem, 1996; 271: 26174-26178
7) Blessing E, Bea F, Kuo CC, Campbell LA, Chesebro B, Rosenfeld ME: Lesion progression and plaque composition are not altered in older apoE-/- mice lacking tumor necrosis factor-alpha receptor p55. Atherosclerosis, 2004; 176: 227-232
8) Zhang L, Peppel K, Sivashanmugam P, Orman ES, Brian L, Exum ST, Freedman NJ: Expression of tumor necrosis factor receptor-1 in arterial wall cells promotes atherosclerosis. Arterioscler Thromb Vasc Biol, 2007; 27: 1087-1094
9) Zhang L, Sivashanmugam P, Wu JH, Brian L, Exum ST, Freedman NJ, Peppel K: Tumor necrosis factor receptor-2 signaling attenuates vein graft neointima formation by promoting endothelial recovery. Arterioscler Thromb Vasc Biol, 2008; 28: 284-289
10) Xanthoulea S, Gijbels MJ, van der Made I, Mujcic H, Thelen M, Vergouwe MN, Ambagts MH, Hofker MH, de Winther MP: P55 tumour necrosis factor receptor in bone marrow-derived cells promotes atherosclerosis development in low-density lipoprotein receptor knock-out mice. Cardiovasc Res, 2008; 80: 309-318
11) Szekanecz Z, Kerekes G, Soltész P: Vascular effects of biologic agents in RA and spondyloarthropathies. Nat Rev Rheumatol, 2009; 5: 677-684
12) Hürlimann D, Forster A, Noll G, Enseleit F, Chenevard R, Distler O, Béchir M, Spieker LE, Neidhart M, Michel BA, Gay RE, Lüscher TF, Gay S, Ruschitzka F: Anti-tumor necrosis factor-alpha treatment improves endothelial function in patients with rheumatoid arthritis. Circulation, 2002; 106: 2184-2187
13) Jacobsson LT, Turesson C, Gülfe A, Kapetanovic MC, Petersson IF, Saxne T, Geborek P: Treatment with tumor necrosis factor blockers is associated with a lower incidence of first cardiovascular events in patients with rheumatoid arthritis. J Rheumatol, 2005; 32: 1213-1218
14) Bongartz T, Sutton AJ, Sweeting MJ, Buchan I, Matteson EL, Montori V: Anti-TNF antibody therapy in rheumatoid arthritis and the risk of serious infections and malignancies: systematic review and meta-analysis of rare harmful effects in randomized controlled trials. JAMA, 2006; 295: 2275-2285
15) Shibata H, Yoshioka Y, Ohkawa A, Minowa K, Mukai Y, Abe Y, Taniai M, Nomura T, Kayamuro H, Nabeshi H, Sugita T, Imai S, Nagano K, Yoshikawa T, Fujita T, Nakagawa S, Yamamoto A, Ohta T, Hayakawa T, Mayumi T,

Vandenabeele P, Aggarwal BB, Nakamura T, Yamagata Y, Tsunoda S, Kamada H, Tsutsumi Y: Creation and X-ray structure analysis of the tumor necrosis factor receptor-1-selective mutant of a tumor necrosis factor-alpha antagonist. J Biol Chem, 2008; 283: 998-1007
16) Yamamoto Y, Tsutsumi Y, Yoshioka Y, Nishibata T, Kobayashi K, Okamoto T, Mukai Y, Shimizu T, Nakagawa S, Nagata S, Mayumi T: Site-specific PEGylation of a lysine- deficient TNF-alpha with full bioactivity. Nat Biotechnol, 2003; 21: 546-552
17) Shibata H, Yoshioka Y, Abe Y, Ohkawa A, Nomura T, Minowa K, Mukai Y, Nakagawa S, Taniai M, Ohta T, Kamada H, Tsunoda S, Tsutsumi Y: The treatment of established murine collagen-induced arthritis with a TNFR1-selective antagonistic mutant TNF. Biomaterials, 2009; 30: 6638-6647
18) Horai R, Asano M, Sudo K, Kanuka H, Suzuki M, Nishihara M, Takahashi M, Iwakura Y: Production of mice deficient in genes for interleukin (IL)-1alpha, IL-1beta, IL-1alpha/beta, and IL-1 receptor antagonist shows that IL-1beta is crucial in turpentine -induced fever development and glucocorticoid secretion. J Exp Med, 1998; 187: 1463-1475
19) Isoda K, Shiigai M, Ishigami N, Matsuki T, Horai R, Nishikawa K, Kusuhara M, Nishida Y, Iwakura Y, Ohsuzu F: Deficiency of interleukin-1 receptor antagonist promotes neointimal formation after injury. Circulation, 2003; 108: 516-518
20) Isoda K, Nishikawa K, Kamezawa Y, Yoshida M, Kusuhara M, Moroi M, Tada N, Ohsuzu F: Osteopontin plays an important role in the development of medial thickening and neointimal formation. Circ Res, 2002; 91: 77-82
21) Isoda K, Sawada S, Ayaori M, Matsuki T, Horai R, Kagata Y, Miyazaki K, Kusuhara M, Okazaki M, Matsubara O, Iwakura Y, Ohsuzu F: Deficiency of interleukin-1 receptor antagonist deteriorates fatty liver and cholesterol metabolism in hypercholesterolemic mice. J Biol Chem, 2005; 280: 7002-7009
22) Usui S, Hara Y, Hosaki S, Okazaki M: A new on-line dual enzymatic method for simultaneous quantification of cholesterol and triglycerides in lipoproteins by HPLC. J Lipid Res, 2002; 43: 805-814
23) Zimmerman MA, Reznikov LL, Sorensen AC, Selzman CH: Relative contribution of the TNF-alpha receptors to murine intimal hyperplasia. Am J Physiol Regul Integr Comp Physiol, 2003; 284: R1213-1218
24) Xanthoulea S, Thelen M, Pöttgens C, Gijbels MJ, Lutgens E, de Winther MP: Absence of p55 TNF receptor reduces atherosclerosis, but has no major effect on angiotensin II induced aneurysms in LDL receptor deficient mice. PLoS One, 2009; 4: e6113
25) Johnston SL, Lock RJ, Gompels MM: Takayasu arteritis: a review. J Clin Pathol, 2002; 55: 481-486
26) Isoda K, Ohsuzu F: The effect of interleukin-1 receptor antagonist on arteries and cholesterol metabolism. J Atheroscler Thromb, 2006; 13: 21-30
27) Matsuki T, Isoda K, Horai R, Nakajima A, Aizawa Y, Suzuki K, Ohsuzu F, Iwakura Y: Involvement of tumor necrosis factor-alpha in the development of T cell-dependent aortitis in interleukin-1 receptor antagonist-deficient mice. Circulation, 2005; 112: 1323-1331
28) Chen G, Goeddel DV: TNF-R1 signaling: a beautiful pathway. Science, 2002; 296: 1634-1635
29) McFarlane SM, Pashmi G, Connell MC, Littlejohn AF, Tucker SJ, Vandenabeele P, MacEwan DJ. Differential activation of nuclear factor-kappaB by tumour necrosis factor receptor subtypes. TNFR1 predominates whereas TNFR2 activates transcription poorly. FEBS Lett, 2002; 515: 119-126
30) Mackay F, Loetscher H, Stueber D, Gehr G, Lesslauer W: Tumor necrosis factor alpha (TNF-alpha)-induced cell adhesion to human endothelial cells is under dominant control of one TNF receptor type, TNF-R55. J Exp Med, 1993; 177: 1277-1286
31) Ip JH, Fuster V, Badimon L, Badimon J, Taubman MB, Chesebro JH: Syndromes of accelerated atherosclerosis: role of vascular injury and smooth muscle cell proliferation. J Am Coll Cardiol, 1990; 15: 1667-1687
32) Ross R: Atherosclerosis--an inflammatory disease. N Engl J Med, 1999; 340: 115-126
33) Zhou Z, Connell MC, MacEwan DJ: TNFR1-induced NF-kappaB, but not ERK, p38MAPK or JNK activation, mediates TNF-induced ICAM-1 and VCAM-1 expression on endothelial cells. Cell Signal, 2007; 19: 1238-1248
34) Collins T, Cybulsky MI: NF-kappa B: pivotal mediator or innocent bystander in atherogenesis? J Clin Invest, 2001; 107: 255-264
35) Pan S, An P, Zhang R, He X, Yin G, Min W: Etk/Bmx as a tumor necrosis factor receptor type 2-specific kinase: role in endothelial cell migration and angiogenesis. Mol Cell Biol, 2002; 22: 7512-7523
36) Smith RA, Baglioni C: The active form of tumor necrosis factor is a trimer. J Biol Chem, 1987; 262: 6951-6954
37) Olleros ML, Guler R, Corazza N, Vesin D, Eugster HP, Marchal G, et al: Transmembrane TNF induces an efficient cell-mediated immunity and resistance to Mycobacterium bovis bacillus Calmette-Guerin infection in the absence of secreted TNF and lymphotoxin-alpha. J Immunol, 2002; 168: 3394-3401
38) Saunders BM, Tran S, Ruuls S, Sedgwick JD, Briscoe H, Britton WJ: Transmembrane TNF is sufficient to initiate cell migration and granuloma formation and provide acute, but not long-term, control of Mycobacterium tuberculosis infection. J Immunol, 2005; 174: 4852-4859

Laboratory of Biopharmaceutical Research[1], National Institute of Biomedical Innovation; Laboratory of Toxicology and Safety Science[2], Graduate School of Pharmaceutical Sciences; The Center for Advanced Medical Engineering and Informatics[3]; Laboratory of Biomedical Innovation[4], Graduate School of Pharmaceutical Sciences, Osaka University, Osaka, Japan

Rho GDP-dissociation inhibitor alpha is associated with cancer metastasis in colon and prostate cancer

T. YAMASHITA[1,2,*], T. OKAMURA[1,*], K. NAGANO[1,*], S. IMAI[1], Y. ABE[1], H. NABESHI[1,2], T. YOSHIKAWA[1,2], Y. YOSHIOKA[1,2,3], H. KAMADA[1,3], Y. TSUTSUMI[1,2,3], S. TSUNODA[1,3,4]

Received July 7, 2011, accepted August 5, 2011

Shin-ichi Tsunoda, Ph.D, Laboratory of Biopharmaceutical Research, National Institute of Biomedical Innovation, 7-6-8 Saito-Asagi, Ibaraki, Osaka 567-0085, Japan.
tsunoda@nibio.go.jp
**These authors contributed equally to the work.*

Pharmazie 67: 253–255 (2012) *doi: 10.1691/ph.2012.1630*

Since metastasis is one of the most important prognostic factors in colorectal cancer, development of new methods to diagnose and prevent metastasis is highly desirable. However, the molecular mechanisms leading to the metastatic phenotype have not been well elucidated. In this study, a proteomics-based search was carried out for metastasis-related proteins in colorectal cancer by analyzing the differential expression of proteins in primary versus metastasis focus-derived colorectal tumor cells. Protein expression profiles were determined using a tissue microarray (TMA), and the results identified Rho GDP-dissociation inhibitor alpha (Rho GDI) as a metastasis-related protein in colon and prostate cancer patients. Consequently, Rho GDI may be useful as a diagnostic biomarker and/or a therapeutic to prevent colon and prostate cancer metastasis.

1. Introduction

Colorectal cancer is known as a major metastatic cancer, and 40–50% of patients already have a metastatic focus at presentation. Moreover, the 5-year survival of these patients is under 10% (Davies et al. 2005). Thus, metastasis is one of the most important prognostic factors in colorectal cancer. In order to improve rates of cancer remission, it will be necessary to clarify the detailed molecular mechanisms of cancer metastasis and to utilize this information to establish new diagnostic and therapeutic techniques. Many researchers have searched for metastasis-related molecules (Liu et al. 2010; Shuehara et al. 2011) using proteomics techniques (Hanash 2003). Comprehensive mapping of the molecular changes during metastasis would greatly improve our understanding of the recurrence and management of cancer. However, the knowledge gained so far in these studies has not been sufficient to improve cancer remission rates.

Here we show the potential of Rho GDI as a metastasis-related protein in colon and prostate cancer patients. In order to identify metastasis-related proteins, the protein expression patterns of human colorectal cancer cells with different metastatic characters were compared. Because these cells were derived from the same patient (SW480: a surgical specimen of a primary colon adenocarcinoma, SW620: a lymph node metastatic focus), cancer metastasis-related protein candidates could be effectively sought without background variations due to differences between individuals. Furthermore, by analyzing the expression of candidate proteins in many clinical samples using a TMA, we attempted to validate the association of these candidates with metastasis. TMA is a slide glass containing many clinical tissues, and it enables one to carry out a high-throughput analysis by evaluating the relationship between expression profiles of each candidate molecule and clinical information such as metastasis. (Imai et al. 2011; Yoshida et al. 2011).

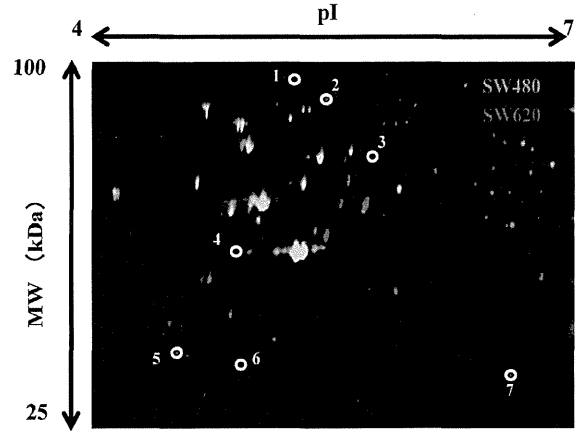

Fig. 1: 2D-DIGE image of fluorescently-labeled proteins from different metastatic human colorectal cancer cells. SW480 is human colorectal cancer cell line derived from a primary tumor and SW620 is derived from a metastatic focus from the same patient. Proteins from the colon cancer cells (SW480, SW620) were labeled with Cy3 and Cy5 respectively, and analyzed by 2D electrophoresis. The differentially-expressed spots (white circles) were then identified by LC-UHR TOF/MS

Table 1: High expression proteins in SW620 compared to SW480

	Accession	Protein name	MW (kDa)	pI	Ratio (SW620 / SW480)
1	P12109	collagen alpha-1(VI) chain	108.6	5.3	1.53
2	Q15459	splicing factor 3A subunit 1	88.9	5.2	1.61
3	P13797	T-plastin	70.9	5.5	1.59
4	P60709	actin cytoplasmic 1	42.1	5.3	1.50
5	P63104	14-3-3 zeta/delta	27.9	4.7	1.63
6	P52565	Rho GDP-dissociation inhibitor 1 (Rho GDI)	23.3	5.0	1.90
7	P30041	Peroxiredoxin-6 (PRDX6)	25.1	6.0	1.86

2. Investigations, results and discussion

In order to search for metastasis-related proteins, we analyzed differentially-expressed proteins between SW480 and SW620 by two-dimensional differential in-gel electrophoresis (2D-DIGE) (Fig. 1). As a result, 7 spots with at least a 1.5-fold-altered expression level were found by quantitative analysis, and these spots were identified by mass spectrometry (Table 1). Three molecules having a high SW620/SW480 expression ratio indicating a strong association with cancer metastasis were identified: Rho GDP-dissociation inhibitor alpha (Rho GDI), peroxiredoxin-6 (PRDX6) and 14-3-3 zeta/delta.

The expression profiles of these proteins were analyzed by immunohistochemistry using the TMA with colon cancer and multiple cancer tissues. Results of this analysis indicated that expression of PRDX6 and 14–3-3 zeta/delta had no relationship to the clinical status of cancer metastasis (data not shown). On the other hand, in positive cases of lymph node metastasis, the expression ratio of Rho GDI was significantly higher than in the negative cases. Furthermore, the same trend was seen when tissues from prostate cancer patients were analyzed (Table 2).

To confirm these results, the expression levels of Rho GDI protein in colon cancer cell lines with different metastatic potential (SW480 < SW620 < SW620-OK1 < SW620-OK2: Characteristics of SW620-OK1 and SW620-OK2 are described in *Experimental*) were investigated by western blot analysis (Fig. 2). The expression of Rho GDI was found to be up-regulated with the development of metastatic characteristics. These results suggested that Rho GDI is correlated with cancer metastasis.

Rho GDI has been identified as key regulator of Rho family GTPases. Activation of growth factor receptors and integrins can promote the exchange of GDP for GTP on Rho proteins (Bishop et al. 2000). Furthermore, GTP-bound Rho proteins interact with a range of effector molecules to modulate their activity or localization, and this leads to changes in cell behavior. It is clear that Rho family GTPases are involved in the control of cell morphology and motility (Etienne-Manneville et al. 2002; Hall et al. 1997; Van Aelst et al. 1997). The importance of Rho protein and Rho GDI in cancer progression, particularly in the area of metastasis, is becoming increasingly evident. Recently, some reports have indicated that the expression of Rho GDI was correlated with colorectal and breast cancer metastasis (Zhao et al. 2008; Kang et al. 2010). Thus, our findings are consistent with these reports and further suggest that the expression of Rho GDI is also correlated with prostate cancer metastasis. Consequently, Rho GDI should be considered as a diagnostic marker or new therapeutic target for cancer metastasis.

3. Experimental

3.1. Cell lines

SW480 is a human colorectal cancer cell line derived from a primary focus and SW620 is derived from a metastatic focus of the same patient. These cells were purchased from American Type Culture Collection and maintained at 37 °C using Leibovitz's L-15 medium (Wako) supplemented with 10% FCS. SW620-OK1 and -OK2 were established by the following procedure: 1×10^6 SW620 cells were injected into the spleens of nu/nu mice. After 8 weeks, SW620-OK1 was established from a liver metastatic focus. Furthermore, SW620-OK2 was established from SW620-OK1 using the same procedures.

3.2. 2D-DIGE analysis

Cell lysates were prepared from SW480 and SW620 and then solubilized with 7 M urea, 2 M thiourea, 4% CHAPS and 10 mM Tris-HCl (pH 8.5). The lysates were labeled at the ratio of 50 μg proteins: 400 pmol Cy3 or Cy5 protein-labeling dye (GE Healthcare Biosciences) in dimethylformamide according to the manufacturer's protocol. Briefly, the labelled samples were mixed with rehydration buffer (7 M urea, 2 M thiourea, 4% CHAPS, 2% DTT, 2% Pharmalyte (GE Healthcare Biosciences)) and applied to a 24-cm immobilized pH gradient gel strip (IPG-strip pH 4–7 NL) for separation in the first dimension. Samples for the spot-picking gel were prepared without labelling by Cy-dyes. For the second dimension separation, the IPG-strips were applied to SDS-PAGE gels (10% polyacrylamide and 2.7% N,N'-diallyltartardiamide gels). After electrophoresis, the gels were scanned with a laser fluoroimager (Typhoon Trio, GE Healthcare Biosciences). The spot-picking gel was scanned after staining with Deep Purple Total Protein Stain (GE Healthcare Biosciences). Quantitative analysis of protein spots was carried out with Decyder-DIA software (GE Healthcare Biosciences). For the antigen spots of interest, spots of 1 mm × 1 mm in size were picked using Ettan Spot Picker (GE Healthcare Biosciences).

3.3. In-gel tryptic digestion

Picked gel pieces were digested with trypsin as described below. The gel pieces were destained with 50% acetonitrile/50 mM NH_4HCO_3 for 20 min twice, dehydrated with 75% acetonitrile for 20 min, and then dried using a centrifugal concentrator. Next, 5 μl of 20 μl/ml trypsin (Promega) solution was added to each gel piece and incubated for 16 h at 37 °C. Three solutions were used to extract the resulting peptide mixtures from the gel pieces. First, 50 μl of 50% (v/v) acetonitrile in 0.1% (v/v) formic acid (FA) was added to the gel pieces, which were then sonicated for 5 min. Next, we collected the solution and added 80% (v/v) acetonitrile in 0.1% FA. Finally, 100% acetonitrile was added for the last extraction. The peptides were dried and then re-suspended in 10 μl of 0.1% FA.

3.4. Mass spectrometry and database search

Extracted peptides were analyzed by liquid chromatography Ultra High Resolution time-of-flight mass spectrometry (LC-UHR TOF/MS; maXis, Bruker Daltonics). The Mascot search engine (http://www.matrixscience.com) was initially used to query the entire theoretical tryptic peptide database as well as SwissProt (http://www.expasy.org/, a public domain database pro-

Table 2: Expression profile of Rho GDI in primary cancers with or without lymph node metastasis

	Number of Rho GDI positive cases (positive ratio)	
	in metastasis negative cases	in metastasis positive cases
Colon cancer*	11/14 (79%)	19/19 (100%)
Prostate cancer*	18/23 (78%)	11/11 (100%)

* $p < 0.05$: Mann Whitney U test

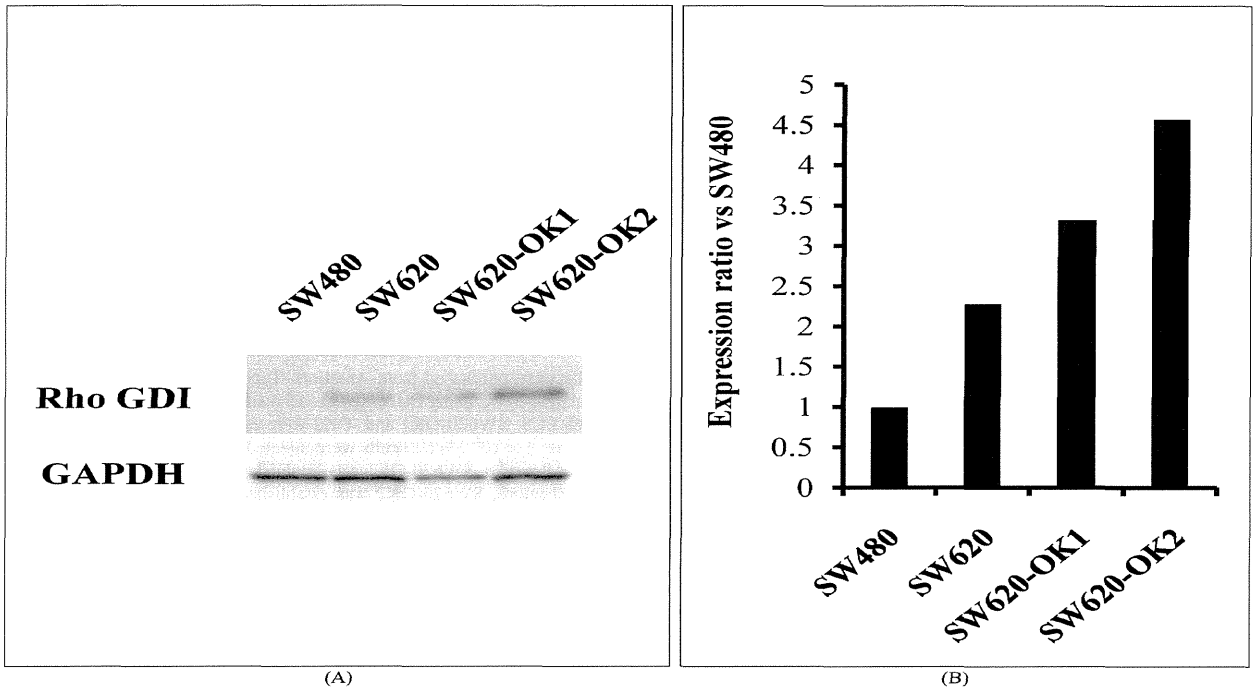

Fig. 2: Rho GDI expression levels in colon cancer cell lines with different metastatic abilities. Rho GDI expression levels in colon cancer cell lines (SW480, SW620, SW620-OK1, SW620-OK2) analyzed by western blotting (A). SW620-OK1, SW620-OK2 have been established as high metastatic sub-lines of SW620 using a mouse metastasis model. Intensity of the western blotting images was quantified by densitometry (B)

vided by the Swiss Institute of Bioinformatics). The search query assumed the following: (i) the peptides were monoisotopic (ii) methionine residues may be oxidized (iii) all cysteines are modified with iodoacetamide.

3.5. TMA Immunochemical staining

TMA slides with human colon cancer samples or multiple cancer samples (Biomax) were de-paraffinated in xylene and rehydrated in a graded series of ethanol washes. Heat-induced epitope retrieval was performed while maintaining the Target Retrieval Solution pH 9 (Dako) at the desired temperature according to manufacturer's instructions. After the treatment, endogenous peroxidase was blocked with 0.3% H_2O_2 in Tris-buffer saline (TBS) for 5 min. After washing twice with TBS, TMA slides were incubated with 10% BSA blocking solution for 30 min. The slides were then incubated with the anti-Rho GDI (Santa Cruz Biotechnology) for 60 min. After washing three times with wash buffer (Dako), each series of sections was incubated for 30 min with Envision + Dual Link (Dako). The reaction products were rinsed twice with wash buffer and then developed in liquid 3, 3'-diaminobenzidine (Dako) for 3 min. After the development, sections were counterstained with Mayer's hematoxylin. All procedures were performed using AutoStainer (Dako).

3.6. TMA Immunohistochemistry scoring

The optimized staining conditions for TMAs corresponding to human colon as well as multiple cancers were determined based on the co-existence of both positive and negative cells in the same tissue sample. Signals were considered positive when reaction products were localized in the expected cellular component. The criteria for scoring of stained tissues were as follows: the distribution score was 0 (0%), 1 (1–50%) or 2 (51–100%), indicating the percentage of positive cells among all tumor cells present in one tissue. The intensity of the signal (intensity score) was scored as 0 (no signal), 1 (weak), 2 (moderate) or 3 (marked). The distribution and intensity scores were then summed into a total score (TS) of TS0 (sum = 0), TS1 (sum = 2), TS2 (sum = 3), and TS3 (sum = 4–5). Throughout this study, TS0 or TS1 was regarded as negative, whereas TS2 or TS3 were regarded as positive.

3.7. Western Blot

Expression of Rho GDI in colon cancer cells was detected by anti-Rho GDI (Santa Cruz Biotechnology) and HRP conjugated anti-mouse IgG antibody (Sigma) using the ECL-plus system. Equal amounts of protein loading were confirmed by parallel β-actin immunoblotting, and signal quantification was performed by densitometric scanning.

Acknowledgements: This study was supported in part by Grants-in-Aid for Scientific Research from the Ministry of Education, Culture, Sports, Science and Technology of Japan, and from the Japan Society for the Promotion of Science (JSPS). This study was also supported in part by Health Labor Sciences Research Grants from the Ministry of Health, Labor and Welfare of Japan.

References

Bishop AL, Hall A (2000) Rho GTPases and their effector proteins. Biochem J 348: 241–255.

Davies RJ, Miller R, Coleman N (2005) Colorectal cancer screening: prospects for molecular stool analysis. Nat Rev Cancer 5: 199–209.

Etienne-Manneville S, Hall A (2002) Rho GTPases in cell biology. Nature 420: 629–635.

Hall A (1997). Rho GTPases and the Actin cytoskeleton. Science 279: 509–514.

Hanash S (2003) Disease proteomics. Nature 422: 226–232.

Imai S, Nagano K, Yoshida Y, Okamura T, Yamashita T, Abe Y, Yoshikawa T, Yoshioka Y, Kamada H, Mukai Y, Nakagawa S, Tsutsumi Y, Tsunoda S (2011). Development of an antibody proteomics system using a phage antibody library for efficient screening of biomarker proteins. Biomaterials 32: 162–169.

Kang S, Kim MJ, An H, Kim BG, Choi YP, Kang KS, Gao MQ, Park H, Na HJ, Kim HK, Yun HR, Kim DS, Cho NH (2010) Proteomic molecular portrait of interface zone in breast cancer. J Proteome Res 9: 5638–5645.

Liu R, Wang K, Yuan K, Wei Y, Huang C (2010) Integrative oncoproteomics strategies for anticancer drug discovery. Expert Rev Proteomics 7: 411–429.

Sahai E (2007). Illuminating the metastatic process. Nat Rev Cancer 7: 737–749.

Suehara Y, Tochigi N, Kubota D, Kikuta K, Nakayama R, Seki K, Yoshida A, Ichikawa H, Hasegawa T, Kaneko K, Chuman H, Beppu Y, Kawai A, Kondo T (2011) Secernin-1 as a novel prognostic biomarker candidate of synovial sarcoma revealed by proteomics. J Proteomics 74: 829–842.

Van Aelst L, D'Souza-Schorey C (1997) Rho GTPases and signaling networks. Genes Dev 11: 2295–2322.

Yoshida Y, Yamashita T, Nagano K, Imai S, Nabeshi H, Yoshikawa T, Yoshioka Y, Abe Y, Kamada H, Tsutsumi Y, Tsunoda S (2011) Limited expression of reticulocalbin-1 in lymphatic endothelial cells in lung tumor but not in normal lung. Biochem Biophys Res Commun 405: 610–614.

Zhao L, Wang H, Li J, Liu Y, Ding Y (2008) Overexpression of Rho GDP-dissociation inhibitor alpha is associated with tumor progression and poor prognosis of colorectal cancer. J Proteome Res 7: 3994–4003.

Biochemical and Biophysical Research Communications 421 (2012) 140–144

Contents lists available at SciVerse ScienceDirect

Biochemical and Biophysical Research Communications

journal homepage: www.elsevier.com/locate/ybbrc

Annexin A4 is a possible biomarker for cisplatin susceptibility of malignant mesothelioma cells

Takuya Yamashita [a,b,1], Kazuya Nagano [a,1], So-ichiro Kanasaki [a,b], Yuka Maeda [a,b], Takeshi Furuya [a,b], Masaki Inoue [a], Hiromi Nabeshi [b], Tomoaki Yoshikawa [a,b], Yasuo Yoshioka [a,b,c], Norio Itoh [b], Yasuhiro Abe [a], Haruhiko Kamada [a,c], Yasuo Tsutsumi [a,b,c], Shin-ichi Tsunoda [a,c,d,*]

[a] Laboratory of Biopharmaceutical Research, National Institute of Biomedical Innovation, 7-6-8 Saito-Asagi, Ibaraki, Osaka 567-0085, Japan
[b] Laboratory of Toxicology and Safety Science, Graduate School of Pharmaceutical Sciences, Osaka University, 1-6 Yamadaoka, Suita, Osaka 565-0871, Japan
[c] The Center for Advanced Medical Engineering and Informatics, Osaka University, 1-6 Yamadaoka, Suita, Osaka 565-0871, Japan
[d] Laboratory of Biomedical Innovation, Graduate School of Pharmaceutical Sciences, Osaka University, 1-6 Yamadaoka, Suita, Osaka 565-0871, Japan

ARTICLE INFO

Article history:
Received 27 March 2012
Available online 4 April 2012

Keywords:
Malignant mesothelioma
Cisplatin susceptibility
Annexin A4
Biomarker
Proteomics

ABSTRACT

Mesothelioma is a highly malignant tumor with a poor prognosis and limited treatment options. Although cisplatin (CDDP) is an effective anticancer drug, its response rate is only 20%. Therefore, discovery of biomarkers is desirable to distinguish the CDDP-susceptible versus resistant cases. To this end, differential proteome analysis was performed to distinguish between mesothelioma cells of different CDDP susceptibilities, and this revealed that expression of annexin A4 (ANXA4) protein was higher in CDDP-resistant cells than in CDDP-susceptible cells. Furthermore, ANXA4 expression levels were higher in human clinical malignant mesothelioma tissues than in benign mesothelioma and normal mesothelial tissues. Finally, increased susceptibility was observed following gene knockdown of ANXA4 in mesothelioma cells, whereas the opposite effect was observed following transfection of an ANXA4 plasmid. These results suggest that ANXA4 has a regulatory function related to the cisplatin susceptibility of mesothelioma cells and that it could be a biomarker for CDDP susceptibility in pathological diagnoses.

1. Introduction

Malignant mesothelioma is an aggressive neoplasm located on serosal membrane surfaces such as the pleura, and less frequently the peritoneum, and it has a poor outcome. The five-year survival rate is only about 5%. On the other hand, it is well known that asbestos is the major causative agent in the development of this disease [1–3]. Moreover, malignant mesothelioma takes 40–50 years to develop following exposure to asbestos. Because of its adiabatic potential, asbestos was commonly used as a building material in the 1960–1970s. Thus, an increase in mesothelioma patients is expected in the future. Patients with pleural malignant mesothelioma commonly present with an effusion associated with breathlessness that is often accompanied by chest-wall pain and a cough. After confirming the diagnosis, many patients are treated by intensive multidirectional approaches that combine cytoreductive surgery with intrapleural or intraperitoneal chemotherapy [4–8]. However, cytoreductive surgery is not always possible for patients with extensive intraperitoneal disease. Thus, the role of chemotherapy in malignant mesothelioma is critically important.

CDDP is an extensively used anticancer drug for the treatment of malignant mesothelioma, although the response rate is only about 20% [9–12]. A major problem with CDDP treatment of malignant mesothelioma patients is the development of CDDP insusceptibility. Thus, there is an urgent need to further our understanding of the pathogenesis of malignant mesothelioma, particularly with respect to the expression of proteins that confer drug susceptibility, in order to develop novel therapeutic strategies. In this study, a proteomic analysis was performed using high- and low-CDDP-susceptible malignant mesothelioma cells to identify candidate proteins associated with CDDP susceptibility.

2. Materials and methods

2.1. Cells

H28, H2052, H2452, H226 and MSTO-221H were purchased from American Type Culture Collection and maintained in RPMI1640 medium (Wako) containing 10% fetal calf serum (Biowest). Human mesothelial cells (HMC) were purchased from

* Corresponding author at: Laboratory of Biopharmaceutical Research, National Institute of Biomedical Innovation, 7-6-8 Saito-Asagi, Ibaraki, Osaka 567-0085, Japan. Fax: +81 72 641 9817.
E-mail address: tsunoda@nibio.go.jp (S.-i. Tsunoda).
[1] These authors contributed equally to this work.

0006-291X/$ - see front matter © 2012 Elsevier Inc. All rights reserved.
http://dx.doi.org/10.1016/j.bbrc.2012.03.144

Sciencell and cultured in Mesothelial Cell Growth Medium (ZenBio) under a 5% CO_2 atmosphere at 37 °C.

2.2. Measurement of cisplatin susceptibility in malignant mesothelioma cells

Malignant mesothelioma cells were seeded into 96-well microplates and cultured overnight. Various concentrations of CDDP were added to each well, the plates were incubated for 24 h, and cell viability was measured using Cell count reagent SF (Nacalai tesque). Absorbance was measured using a microplate reader (Bio-Rad) at test and reference wavelengths of 450 and 650 nm, respectively.

2.3. Proteomic analysis using two dimensional differential in-gel electrophoresis

For proteomic analysis, quantitative analysis was performed using two dimensional differential in-gel electrophoresis (2D-DIGE). Cell lysates were prepared from H28 and H2052 and then solubilized with 7 M urea, 2 M thiourea, 4% CHAPS and 10 mM Tris–HCl (pH 8.5). The lysates were labeled at the ratio of 50 μg proteins: 400 pmol Cy3 or Cy5 protein-labeling dye (GE Healthcare Biosciences) in dimethylformamide according to the manufacturer's protocol. The labelled samples were mixed with rehydration buffer (7 M urea, 2 M thiourea, 4% CHAPS, 2% DTT, 2% Pharmalyte (GE Healthcare Biosciences)) and applied to a 24-cm immobilized pH gradient gel strip (IPG-strip pH 4–7) for separation in the first dimension. For the second dimension separation, the IPG-strips were treated with iodoacetamide and applied to SDS-PAGE gels (10% polyacrylamide and 2.7% *N,N′*-diallyltartardiamide gels). After electrophoresis, the gels were scanned with a laser fluoroimager (Typhoon Trio, GE Healthcare Biosciences). The spot-picking gel was scanned after staining with Deep purple total protein stain (GE Healthcare Biosciences). Quantitative analysis of protein spots was carried out with Decyder-DIA software (GE Healthcare Biosciences). For the antigen spots of interest, spots of 1 mm × 1 mm in size were picked using Ettan Spot Picker (GE Healthcare Biosciences).

2.4. In-gel tryptic digestion

Picked gel pieces were destained with 50% acetonitrile/50 mM NH_4HCO_3 for 20 min twice, dehydrated with 75% acetonitrile for 20 min, and then dried using a centrifugal concentrator. Five microliter of 20 μg/ml trypsin (Promega) solution was added to each gel piece and the pieces were incubated for 16 h at 37 °C. The digested peptides were extracted sequentially using 50%, 80%, and 100% acetonitrile and then dried before being suspended in 10 μl of 0.1% formic acid.

2.5. Mass spectrometry and database search

Extracted peptides were analyzed by liquid chromatography ultra high resolution time-of-flight mass spectrometry (LC-UHR TOF-MS/MS; maXis, Bruker Daltonics). The Mascot search engine (http://www.matrixscience.com) was initially used to query the entire theoretical tryptic peptide database as well as SwissProt (http://www.expasy.org/, a public domain database provided by the Swiss Institute of Bioinformatics). The search query assumed the following: (i) the peptides were mono-, di- or tri-isotopic, (ii) methionine residues may be oxidized, (iii) all cysteines were modified with carbamidomethyl.

2.6. Western blot

The cell lysates were separated in 10% SDS–polyacrylamide gels and transferred to Immobilon membranes (Millipore). After blocking by 4% block ace (DS Pharma Biomedical) for 1 h at room temperature, the blots were reacted with primary antibodies in a buffer containing 0.4% block ace, and then with the appropriate peroxidase-conjugated secondary antibodies in the same buffer. Expression of ANXA4 in malignant mesothelioma cells was detected by mouse anti-human ANXA4 (Abnova: 1D3) followed by an HRP-conjugated anti-mouse IgG antibody (Sigma–Aldrich) using the ECL-plus system (GE Healthcare Biosciences). Equal amounts of protein loading were confirmed by parallel β-actin immunoblotting, and signal quantification was performed by densitometric scanning.

2.7. Immunohistochemistry staining

Human mesothelioma and normal tissue sections were deparaffinated in xylene and rehydrated in a graded series of ethanol dilutions. Heat-induced epitope retrieval was performed by incubating at different temperatures following the manufacturer's instructions using Target Retrieval Solution pH 9 (Dako). After heat-induced epitope retrieval treatment, endogenous peroxidase was blocked with a peroxidase blocking reagent (Dako). Following peroxidase blocking, the slides were incubated with 10% bovine serum albumin (BSA) solution for 30 min at room temperature. The slides were then incubated for 60 min with anti-human ANXA4 monoclonal antibody (9 μg/ml) in 3% BSA at room temperature. After washing 3 times with wash buffer (Dako), the slides were incubated for 30 min with ENVISION + Dual Link (Dako) at room temperature. They were then washed final 3 times and stained with 3,3′-diaminobenzidine. After development, the slides were lightly counterstained with Mayer's hematoxylin and mounted with resinous mounting medium.

2.8. Cisplatin susceptibility in cells transfected with ANXA4-siRNA and ANXA4-plasmid

H28 was transfected with ANXA4-siRNA (target sequence: AAGGATATCACAGAAGGATAT, Qiagen) using Hyperfect reagent (Qiagen) according to the manufacturer's instructions. In contrast, H2052 was transfected with ANXA4-pcDNA 3.1 (a gift from Naka T: Laboratory for Immune Signal, National Institute of Biomedical Innovation) using FuGENE HD transfection reagent (Roche). After transfection, the cells were treated with various concentrations of CDDP for 36 h (ANXA4-siRNA) or 24 h (ANXA4-pcDNA 3.1). Cell viability was measured as described above.

2.9. Statistical analysis

Differences in tumor volumes between the control and target groups were compared using the unpaired Student's *t*-test.

3. Results

3.1. CDDP susceptibility in malignant mesothelioma cells

Cell viability following CDDP treatment was examined to determine which cell lines had higher or lower susceptibility to CDDP. Among five tested mesothelioma cell lines, H2052 was the most and H28 the least susceptible cell line (Fig. 1). The IC_{50} values of H28, H2052, H2452, H226 and MSTO-221H were 154.5, 27.8, 66.0, 87.5 and 49.5 μM, respectively.

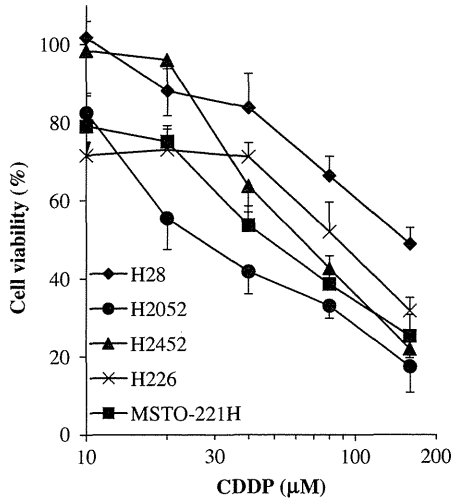

Fig. 1. Susceptibility of malignant mesothelioma cells to CDDP. Mesothelioma cells, H28, H2052, H2452, H226 and MSTO-221H were cultured with various concentrations of CDDP for 24 h 37 °C under 5% CO_2. Cell viability was assayed using the WST-8 assay. Maximal cell viability (100%) was obtained by incubating cells without CDDP. Data are shown as means and standard deviations ($n = 4$).

3.2. Identification of differentially expressed proteins by 2D-DIGE and MS

In order to search for CDDP susceptibility-related proteins, differential proteome analysis between H2052 and H28 cell lines was performed to search for CDDP susceptibility-related proteins (Fig. 2). Quantitative image analysis indicated that a total of eight protein spots representing > 2.0-fold alteration in expression were found and then identified by MS analysis (Table 1). Among those eight proteins, we focused on ANXA4 because this protein plays an important role in membrane stability. Previous reports have indicated that ANXA4 is associated with chemoresistance against platinum-based anticancer drugs in human lung, colon [13] and ovarian cancer [14].

3.3. ANXA4 expression analysis in human malignant mesothelioma cells and mesothelial tissues

Correlations between the expression levels in five malignant mesothelioma cell lines with CDDP-susceptibility were examined using western blot analysis to validate the identified proteins as CDDP susceptibility-related proteins. ANXA4 was expressed at a higher level in H28 cells relative to the other four CDDP-susceptible malignant mesothelioma cell lines (Fig. 3A and B). Expression of ANXA4 in human mesothelial tissue was analyzed by immunohistochemistry staining with an anti-human ANXA4 monoclonal antibody. Fig. 3C indicates that ANXA4 was expressed at higher levels in human malignant mesothelioma tissues than in benign mesothelioma tissues and normal mesothelial tissues.

3.4. Gene regulation of ANXA4 in malignant mesothelioma cells by knockdown and overexpression

ANXA4-siRNA and ANXA4-pcDNA 3.1 were next transfected to H28 and H2052 before CDDP treatment to evaluate correlations between ANXA4 expression levels and CDDP susceptibility. The IC_{50} values of [H28/non treat: H28/control-siRNA: H28/ANXA4-siRNA] were [80.0 μM: 71.8 μM: 15.5 μM] and [H2052/control-pcDNA 3.1: [H2052/ANXA4-pcDNA 3.1] were [55.2 μM: 89.7 μM], respectively (Fig. 4A–D). These results suggested that the CDDP susceptibility of H28 cells was increased by ANXA4-siRNA transfection and that of H2052 cells was decreased by ANXA4-pcDNA 3.1 transfection.

4. Discussion

In this study, a proteomic analysis was performed based on 2D-DIGE using malignant mesothelioma cell lines to identify candidate proteins associated with CDDP susceptibility (Figs. 1 and 2). Eight proteins that were differentially expressed in H28 cells compared with H2052 cells were identified (Table 1). ANXA4 was found to be expressed at a higher level in H28 cells relative to levels in CDDP-susceptible malignant mesothelioma cells by western blot

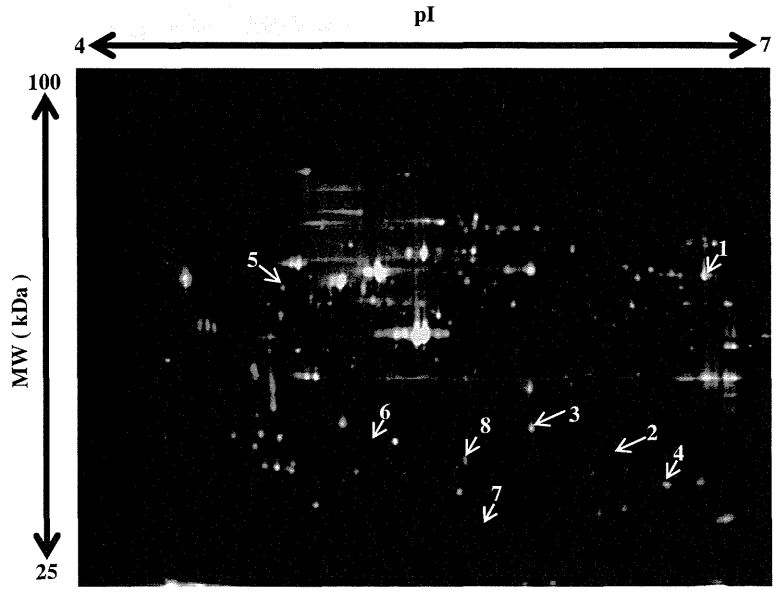

Fig. 2. 2D-DIGE image of fluorescently labeled proteins from human mesothelioma cell lines H28 and H2052. Proteins from high- and low-susceptible mesothelioma cells (H2052, H28) were labeled with cy3 and cy5, respectively, and 2D electrophoresis was performed. The differentially expressed spots in H28 indicated by white arrows were then identified by LC-TOF-MS/MS. Table 1 contains additional information about the identified proteins.

Table 1
Proteins expressed at higher or lower levels in H28 compared to H2052.

No.	Accession number	Protein name	pI	MW (kDa)	Expression ratio (H28/H2052)
1	P11413	Glucose-6-phosphate 1-dehydrogenase	6.4	59.3	21.0
2	P78417	Glutathione *S*-transferase omega-1	6.2	27.6	7.4
3	P09525	Annexin A4	5.6	35.9	3.6
4	P30041	Peroxiredoxin-6	6.0	25.0	3.5
5	Q09028	Histone-binding protein RBBP4	4.7	47.7	3.0
6	P07195	*L*-lactate dehydrogenase B chain	5.7	36.6	2.9
7	P32119	Peroxiredoxin-2	5.7	21.9	0.03
8	Q9Y696	Chloride intracellular channel protein 4	5.5	28.8	0.13

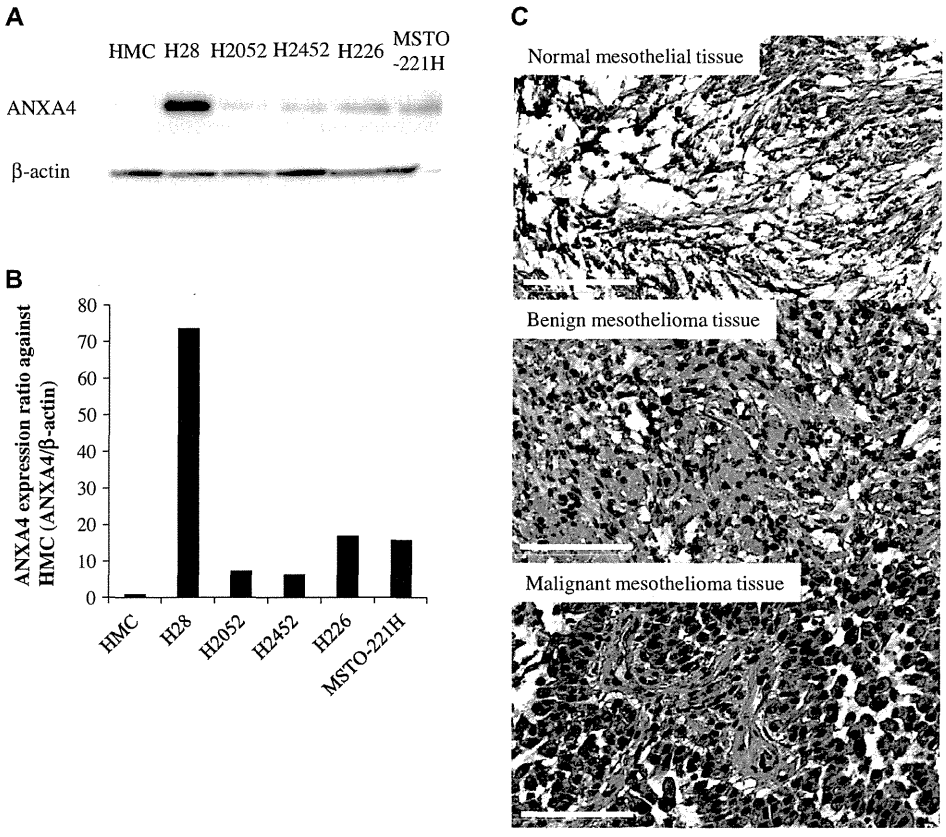

Fig. 3. ANXA4 expression analysis in human malignant mesothelioma cells and mesothelial tissues. ANXA4 expression levels in human primary mesothelial cells, HMC, and mesothelioma cell lines (H28, H2052, H2452, H226, MSTO-221H) were analyzed by western blotting (A). Intensity of the western blotting images was quantified by densitometry (B). Expression of ANXA4 in human mesothelial tissues was analyzed by immunostaining using an anti-human ANXA4 antibody (C). Top, middle and bottom panels are normal mesothelial, benign and malignant mesothelioma tissues, respectively. The tissue sections were counterstained using hematoxylin. Representative 400 × photomicrographs presented (bar: 100 μm).

analysis (Fig. 3A and B). Furthermore, ANXA4 was expressed in malignant mesothelioma tissue but not in benign mesothelial tumor and normal mesothelial tissues (Fig. 3C). Thus, ANXA4 was expressed in CDDP-susceptible malignant mesothelioma cells and specifically in malignant mesothelioma tissues. These results indicate that ANXA4 expression in malignant mesothelioma cells may be correlated with CDDP susceptibility, although this relationship must be validated in future studies of human clinical malignant mesothelial cases. The CDDP susceptibility of H28 cells was actually increased by ANXA4 knockdown, and that of H2052 cells was decreased by ANXA4 overexpression (Fig. 4). Thus, these results suggest that ANXA4 plays an important role in chemoresistance against CDDP.

ANXA4 has already been characterized as a regulator of cell membranes with calcium dependency [15–17]. Recently, some studies have reported the protein is associated with membrane permeability [18], ion channels [19] and exocytosis [20,21]. These observations may explain in part the correlation of ANXA4 with modulation of drug susceptibility in cancer cells.

This study demonstrates for the first time elevated ANXA4 protein expression in malignant mesothelioma cells that have less susceptibility to CDDP. *In vitro* evaluation of drug susceptibility against CDDP in malignant mesothelioma cells derived from cancer patients would be important in clinical conditions because doctors as well as patients wish to avoid treatment with inefficacious drugs. Consequently, the susceptibility of a given patient against CDDP could be confirmed by analyzing the expression level of ANXA4 in malignant mesothelioma patients at the time of diagnosis. Furthermore, if ANXA4 expression could be blocked specifically in malignant mesothelioma cells by nucleic acid drugs such as siRNA, this procedure would prove useful in clinical situations involving CDDP treatment. The present study may contribute to

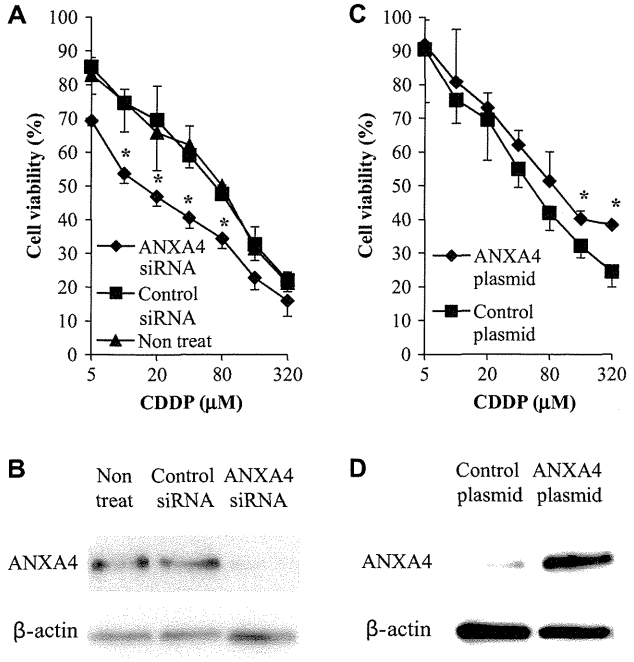

Fig. 4. The effect of ANXA4 gene knockdown and overexpression on CDDP susceptibility in malignant mesothelioma cells. Transfection of ANXA4 siRNA or plasmid into malignant mesothelioma cells confers resistance to CDDP. Cell survival after 24 h treatment of H28/ANXA4 siRNA or H2052/ANXA4 plasmid with different concentrations of CDDP (A and C). Expression of ANXA4 was analyzed by western blot analysis (B and D). Data are shown as means and standard deviations ($n = 4$). *$P < 0.05$ (Control siRNA or plasmid vs. ANXA4 siRNA or plasmid).

establishment of a new therapeutic strategy for malignant mesothelioma patients by suggesting a novel diagnostic and therapeutic target.

Acknowledgments

This study was supported in part by Grants-in-Aid for Scientific Research from the Ministry of Education, Culture, Sports, Science and Technology of Japan, and from the Japan Society for the Promotion of Science (JSPS). This study was also supported in part by Health Labor Sciences Research Grants from the Ministry of Health, Labor and Welfare of Japan and by Health Sciences Research Grants for Research on Publicly Essential Drugs and Medical Devices from the Japan Health Sciences Foundation.

References

[1] W.N. Rom, W.D. Travis, A.R. Brody, Cellular and molecular basis of the asbestos-related diseases, Am. Rev. Respir. Dis. 143 (1991) 408–422.
[2] N.H. Heintz, Y.M. Janssen-Heininger, B.T. Mossman, Asbestos, lung cancers, and mesotheliomas: from molecular approaches to targeting tumor survival pathways, Am. J. Respir. Cell Mol. Biol. 42 (2010) 133–139.
[3] Consensus Report: Asbestos, asbestosis, and cancer: the Helsinki criteria for diagnosis and attribution. Scand. J. Work Environ. Health 23 (1997) 311–316.
[4] T.D. Yan, L. Welch, D. Black, P.H. Sugarbaker, A systematic review on the efficacy of cytoreductive surgery combined with perioperative intraperitoneal chemotherapy for diffuse malignancy peritoneal mesothelioma, Ann. Oncol. 18 (2007) 827–834.
[5] E. Chailleux, D. Pioche, S. Chopra, G. Dabouis, P. Germaud, A.Y. De Lajartre, M. De Lajartre, Prognostic factors in diffuse malignant pleural mesothelioma: a study of 167 patients, Chest 93 (1988) 159–162.
[6] K.S. Sridhar, R. Doria, W.A. Raub Jr., R.J. Thurer, M. Saldana, New strategies are needed in diffuse malignant mesothelioma, Cancer 70 (1992) 2969–2979.
[7] M. Markman, D. Kelsen, Efficacy of cisplatin-based intraperitoneal chemotherapy as treatment of malignant peritoneal mesothelioma, J. Cancer Res. Clin. Oncol. 118 (1992) 547–550.
[8] G.H. Eltabbakh, M.S. Piver, R.E. Hempling, F.O. Recio, M.E. Intengen, Clinical picture, response to therapy, and survival of women with diffuse malignant peritoneal mesothelioma, J. Surg. Oncol. 70 (1999) 6–12.
[9] T. Berghmans, M. Paesmans, Y. Lalami, I. Louviaux, S. Luce, C. Mascaux, A.P. Meert, J.P. Sculier, Activity of chemotherapy and immunotherapy on malignant mesothelioma: a systematic review of the literature with meta-analysis, Lung. Cancer 38 (2002) 111–121.
[10] H.J. Lerner, D.A. Schoenfeld, A. Martin, G. Falkson, E. Borden, Malignant mesothelioma: The Eastern Cooperative Oncology Group (ECOG) experience, Cancer 52 (1983) 1981–1985.
[11] D.M. Mintzer, D. Kelsen, D. Frimmer, R. Heelan, R. Gralla, Phase II trial of high-dose cisplatin in patients with malignant mesothelioma, Cancer Treat Rep. 69 (1985) 711–712.
[12] B.L. Zidar, S. Green, H.I. Pierce, R.W. Roach, S.P. Balcerzak, L. Militello, A phase II evaluation of cisplatin in unresectable diffuse malignant mesothelioma: a Southwest Oncology Group Study, Invest New Drugs 6 (1988) 223–226.
[13] E.K. Han, S.K. Tahir, S.P. Cherian, N. Collins, S.C. Ng, Modulation of paclitaxel resistance by annexin IV in human cancer cell lines, Br. J. Cancer 83 (2000) 83–88.
[14] A. Kim, T. Enomoto, S. Serada, Y. Ueda, T. Takahashi, B. Ripley, T. Miyatake, M. Fujita, C.M. Lee, K. Morimoto, M. Fujimoto, T. Kimura, T. Naka, Enhanced expression of Annexin A4 in clear cell carcinoma of the ovary and its association with chemoresistance to carboplatin, Int. J. Cancer 125 (2009) 2316–2322.
[15] M.A. Kaetzel, P. Hazarika, J.R. Dedman, Differential tissue expression of three 35-kDa annexin calcium-dependent phospholipid-binding proteins, J. Biol. Chem. 264 (1989) 14463–14470.
[16] G. Zanotti, G. Malpeli, F. Gliubich, C. Folli, M. Stoppini, L. Olivi, A. Savoia, R. Berni, Structure of the trigonal crystal form of bovine annexin IV, Biochem. J. 329 (1998) 101–106.
[17] M.A. Kaetzel, Y.D. Mo, T.R. Mealy, B. Campos, W. Bergsma-Schutter, A. Brisson, J.R. Dedman, B.A. Seaton, Phosphorylation mutants elucidate the mechanism of annexin IV-mediated membrane aggregation, Biochemistry 40 (2001) 4192–4199.
[18] W.G. Hill, M.A. Kaetzel, B.K. Kishore, J.R. Dedman, M.L. Zeidel, Annexin A4 reduces water and proton permeability of model membranes but does not alter aquaporin 2-mediated water transport in isolated endosomes, J. Gen. Physiol. 121 (2003) 413–425.
[19] M.A. Kaetzel, H.C. Chan, W.P. Dubinsky, J.R. Dedman, D.J. Nelson, A role for annexin IV in epithelial cell function. Inhibition of calcium-activated chloride conductance, J. Biol. Chem. 269 (1994) 5297–5302.
[20] H. Sohma, C.E. Creutz, S. Gasa, H. Ohkawa, T. Akino, Y. Kuroki, Differential lipid specificities of the repeated domains of annexin IV, Biochim. Biophys. Acta 1546 (2001) 205–215.
[21] A. Piljic, C. Schultz, Annexin A4 self-association modulates general membrane protein mobility in living cells, Mol. Biol. Cell 17 (2006) 3318–3328.

Cytokine 61 (2013) 578–584

Contents lists available at SciVerse ScienceDirect

Cytokine

journal homepage: www.journals.elsevier.com/cytokine

Mutants of lymphotoxin-α with augmented cytotoxic activity *via* TNFR1 for use in cancer therapy

Tomohiro Morishige [a,1], Yasuo Yoshioka [b,c,*,1], Shogo Narimatsu [a], Shinji Ikemizu [d], Shin-ichi Tsunoda [c,e], Yasuo Tsutsumi [b,c,e], Yohei Mukai [a], Naoki Okada [a], Shinsaku Nakagawa [a,c,*]

[a] *Laboratory of Biotechnology and Therapeutics, Graduate School of Pharmaceutical Sciences, Osaka University, 1-6 Yamadaoka, Suita, Osaka 565-0871, Japan*
[b] *Laboratory of Toxicology and Safety Science, Graduate School of Pharmaceutical Sciences, Osaka University, 1-6 Yamadaoka, Suita, Osaka 565-0871, Japan*
[c] *The Center for Advanced Medical Engineering and Informatics, Osaka University, 1-6 Yamadaoka, Suita, Osaka 565-0871, Japan*
[d] *Graduate School of Pharmaceutical Sciences, Kumamoto University, 5-1 Oe-honmachi, Kumamoto 862-0973, Japan*
[e] *Laboratory of Biopharmaceutical Research, National Institute of Biomedical Innovation, 7-6-8 Saito-Asagi, Ibaraki, Osaka 567-0085, Japan*

ARTICLE INFO

Article history:
Received 6 July 2012
Received in revised form 29 September 2012
Accepted 6 November 2012
Available online 11 December 2012

Keywords:
Affinity
Apoptosis
Bioactivity
Cytokine
Cytotoxicity

ABSTRACT

The cytokine lymphotoxin-α (LTα) is a promising candidate for use in cancer therapy. However, the instability of LTα *in vivo* and the insufficient levels of tumor necrosis factor receptor 1 (TNFR1)-mediated bioactivity of LTα limit its therapeutic potential. Here, we created LTα mutants with increased TNFR1-mediated bioactivity by using a phage display technique. We constructed a phage library displaying lysine-deficient structural variants of LTα with randomized amino acid residues. After affinity panning, we screened three clones of lysine-deficient LTα mutant, and identified a LTα mutant with TNFR1-mediated bioactivity that was 32 times that of the wild-type LTα (wtLTα). When compared with wtLTα, the selected clone showed augmented affinity to TNFR1 due to slow dissociation rather than rapid association. In contrast, the mutant showed only 4 times the TNFR2-mediated activity of wtLTα. In addition, the LTα mutant strongly and rapidly activated caspases that induce TNFR1-mediated cell death, whereas the mutant and wtLTα activated nuclear factor-kappa B to a similar extent. Our data suggest that the kinetics of LTα binding to TNFR1 play an important role in signal transduction patterns, and a TNFR1-selective LTα mutant with augmented bioactivity would be a superior candidate for cancer therapy.

1. Introduction

Lymphotoxin-alpha (LTα) is a tumor necrosis factor (TNF) superfamily cytokine with tumor-cell-specific cytotoxic activity and immune-activating activity. LTα induces the expression of chemokines and adhesion molecules in endothelial cells, and plays a key role in lymph node neogenesis [1–3]. Schrama et al. [4,5] showed that systemic administration of LTα to a tumor-bearing mouse leads to the construction of ectopic lymphoid tissue within the tumor and the strong induction of tumor immunity in that lymphoid tissue, suggesting that the underlying mechanism of this cytokine's anti-tumor activity may be effective. Therefore, LTα has long been considered to be a promising candidate for an anti-cancer agent. However, the clinical use of LTα has been limited because of the protein's *in vivo* instability and proinflammatory side effects.

One of the most common ways to improve the therapeutic effects of proteins is to conjugate them with polyethylene glycol (PEG) in a process called PEGylation, or to conjugate them with other water-soluble polymers [6]. Because of the steric hindrance caused by the PEG molecule, PEGylation can prolong the plasma half-life of molecules and alter the tissue distribution of the conjugates compared with those of the native form. PEGylation of proteins is mostly nonspecific because it targets all of the lysine residues in the protein, some of which may be in or near an active site. As a result, PEGylation significantly reduces the specific

Abbreviations: E. coli, Escherichia coli; ELISA, enzyme-linked immunosorbent assay; FADD, Fas-associated protein with death domain; FBS, fetal bovine serum; HVEM, herpes virus entry mediator; IFNγ, interferon γ; LTα, lymphotoxin-alpha; NFκB, nuclear factor-kappa B; PEG, polyethylene glycol; pI, isoelectric points; SDS–PAGE, sodium dodecyl sulfate–polyacrylamidegel electrophoresis; SPR, surface plasmon resonance; TNF, tumor necrosis factor; TNFR1, TNF receptor 1; TRADD, TNF receptor-associated death domain; TRAF, TNF receptor-associated factor; wtLTα, wild-type LTα.

* Corresponding authors. Addresses: Laboratory of Toxicology and Safety Science, Graduate School of Pharmaceutical Sciences, Osaka University, 1-6 Yamadaoka, Suita, Osaka 565-0871, Japan. Tel./fax: +81 6 6879 8233 (Y. Yoshioka), Laboratory of Biotechnology and Therapeutics, Graduate School of Pharmaceutical Sciences, Osaka University, 1-6 Yamadaoka, Suita, Osaka 565-0871, Japan. Tel.: +81 6 6879 8175; fax: +81 6 6879 8179 (S. Nakagawa).

E-mail addresses: yasuo@phs.osaka-u.ac.jp (Y. Yoshiokab), nakagawa@phs.osaka-u.ac.jp (S. Nakagawa).

[1] These authors contributed equally to the work.

1043-4666/$ - see front matter © 2012 Elsevier Ltd. All rights reserved.
http://dx.doi.org/10.1016/j.cyto.2012.11.005

activity of the proteins involved. Our group previously developed a novel strategy for site-specific mono-PEGylation of lysine-deficient mutants to overcome these limitations of PEGylation [7,8]. We demonstrated that site-specific PEGylation of a lysine-deficient mutant of LTα retained higher bioactivity compared with random PEGylation of wild-type LTα (wtLTα) [9]. This finding suggests that site-specific PEGylation of a lysine-deficient mutant of LTα might be a useful way to overcome the problems in the clinical use of LTα outlined above.

LTα binds to three receptor subtypes—TNF receptor 1 (TNFR1), TNFR2, and herpes virus entry mediator (HVEM)—to exert various biological functions. TNFR1 induces an anti-tumor effect and Peyer's patch development, whereas TNFR2 is essential for immune responses against bacteria and viruses [1]. Human LTα and TNF that bind to murine TNFR1, but not to murine TNFR2, are not lethal in healthy mice except at extremely high doses, suggesting that LTα and TNF α exhibit their lethal side effects *via* TNFR2 [10,11]. Therefore, LTα as a cancer immunotherapeutic agent, a LTα mutant with selectively increased TNFR1-mediated bioactivity is needed. Previously, we successfully created a TNFR1-selective LTα mutant whose bioactivity *via* TNFR1 was several times that of wtLTα, and whose bioactivity *via* TNFR2 was 2.5% that of wtLTα [12]. However, to enhance therapeutic efficacy and suppress the side effect of LTα, it is necessary to create a LTα mutant with greatly increased TNFR1-mediated bioactivity and TNFR1-selectivity.

In this study, we attempted to create LTα mutants with selectively increased TNFR1-mediated bioactivity by using a phage display technique. We succeeded in creating a LTα mutant that had a much higher bioactivity *via* TNFR1 and an augmented affinity to TNFR1 compared with that of wtLTα, and demonstrated that this was due to the slow dissociation rate of the LTα mutant-TNFR1 complex. In addition, we showed that the LTα mutant differed from wtLTα by its ability to strongly and rapidly activate caspases. In contrast, the LTα mutant and wtLTα were similar to each other in their degree of activation of nuclear factor-kappa B (NFκB). Our findings suggest that this LTα mutant would be a superior candidate for a cancer immunotherapeutic agent.

2. Materials and methods

2.1. Cells

HEp-2 cells, a human carcinoma cell line derived via HeLa contamination, were purchased from the American Type Culture Collection (Manassas, VA), and cultured in RPMI 1640 medium (Wako Pure Chemical Industries, Osaka, Japan) supplemented with 10% fetal bovine serum (FBS), 1 mM sodium pyruvate, 50 μM 2-mercaptoethanol, and antibiotics. HT29.14S cells, a TNF/LT-sensitive subclone of HT29 human colon adenocarcinoma, were kindly provided by Dr. Carl Ware (La Jolla Institute for Allergy and Immunology, CA) [13]. HT29.14S cells were cultured in Dulbecco's Modified Eagle's Medium (Wako Pure Chemical Industries) supplemented with 10% FBS, 10 mM HEPES, and antibiotics. hTNFR2/mFas-PA cells are preadipocytes derived from TNFR1$^{-/-}$ TNFR2$^{-/-}$ mice expressing a chimeric receptor composed of the extracellular and transmembrane domain of human TNFR2 and the intracellular domain of mouse Fas, which is a member of the TNF receptor superfamily [14]; these cells were cultured in RPMI 1640 medium supplemented with 10% FBS, 5 μg/mL Blasticidin S HCl (Invitrogen, Carlsbad, CA), and antibiotics. MCF-7 cells were provided from the Institute of Development, Aging and Cancer, Tohoku University, and were cultured in Eagle's Minimum Essential Medium (Wako Pure Chemical Industries) supplemented with 10% FBS, 0.01 mg/mL bovine insulin, and antibiotics.

2.2. Construction of a library of lysine-deficient mutants of LTα

The phagemid vector pY03′, which encodes human wtLTα with the C-terminus of wtLTα fused to the N-terminus of the M13 phage g3p, was used as a PCR template for constructing a DNA library of lysine-deficient mutants of LTα. We performed a two-step PCR amplification using oligonucleotides containing the sequence NNS (where N represents A, C, G, or T; and S represents C or G) at Lys19, Lys28, Lys39, Lys84, Lys89, and Lys119 of wtLTα; the sequence NNS encodes all 20 standard amino acids. The products from the second PCR were digested with *NcoI* and *PstI* and then ligated into pY03′. The phagemid was electroporated into *Escherichia coli* (*E. coli*) TG1 cells (Stratagene, Cedar Creek, TX), yielding 2×10^6 independent clones. The phage library displaying lysine-deficient LTα molecules was prepared as described previously [12]. Briefly, pY03′-transformed TG1 cells were infected with M13KO7 helper phage (Invitrogen) and cultured for 6 h at 25 °C. The resultant phage particles were precipitated from the culture supernatant by using PEG (MP Biomedicals, Solon, OH) and suspended in NTE (100 mM NaCl, 10 mM Tris, 1 mM EDTA).

2.3. Selection of bioactive LTα mutants

Screening for bioactive LTα mutants was performed as described previously [12]. Briefly, an immunoplate was coated with soluble human TNFR1 (R&D Systems, Minneapolis, MN), and the prepared phage library was allowed to bind to the immobilized TNFR1. After a second round of panning, single colonies were picked and cultured. The resulting phage-containing culture supernatant was used for screening by enzyme-linked immunosorbent assay (ELISA) against human TNFR1.

2.4. Expression and purification of recombinant LTαs

pET15b plasmids (Novagen, Darmstadt, Germany) encoding LTαs were prepared and used to transform *E. coli* BL21(DE3) cells (Stratagene) for the expression of recombinant protein, as described previously [12]. Expression was induced by adding 1 mM isopropyl β-D-1-thiogalactopyranoside and incubating the cells at 37 °C for 6 h in Terrific Broth (Invitrogen Corporation, Carlsbad, CA) containing 0.4% glucose, 1.68 mM $MgSO_4$, and 100 μg/mL of ampicillin; all products were accumulated as inclusion bodies. The resultant inclusion bodies were washed, solubilized, reduced, and refolded by the methods previously described [12]. After dialysis against a buffer containing 20 mM Tris–HCl (pH 7.4) and 100 mM urea, active trimeric LTα proteins were purified by using a HiLoad Superdex 200PG column (GE Healthcare, UK) equilibrated with phosphate-buffered saline (pH 7.4) followed by ion-exchange chromatography (SP Sepharose Fast Flow for wtLTα; Q Sepharose Fast Flow for mutants of LTα); both columns were obtained from GE Healthcare. To create point mutants, we used pET15b-human wtLTα as a template with a KOD-plus mutagenesis kit (Toyobo, Osaka, Japan) according to the manufacturer's instructions. Recombinant point mutants were produced and purified as described earlier; SP Sepharose Fast Flow was used as the ion-exchange column. Protein concentration was measured by using Coomassie Protein Assay Reagent (Thermo Fisher Scientific, Rockford, IL). Sodium dodecyl sulfate–polyacrylamidegel electrophoresis (SDS–PAGE) analysis of LTαs was conducted under reducing conditions, and the proteins in the gels were stained with Coomassie brilliant blue. The electrostatic potential surface was generated by using GRASP software [15]. The electrostatic potential ranged from −7.5 kT to 7.5 kT. The relative accessible surface areas were calculated by using JOY software [16].

2.5. Cytotoxicity assays

HEp-2 cells were seeded at 4×10^4 cells per well in 96-well plates and incubated for 18 h with serially-diluted LTαs in the presence of 50 μg/mL cycloheximide. For the functional blocking assay, HEp-2 cells were treated with serially-diluted MAB225 (R&D Systems), an anti-TNFR1 antibody, for 30 min. The cells were then incubated with 100 ng/mL wtLTα and LTα mutants for 18 h in the presence of 50 μg/mL cycloheximide. For the caspase inhibition assay, HEp-2 cells were incubated with serially-diluted wtLTα or LTα mutants in the presence of 50 μg/mL cycloheximide and 50 mM zVAD-fmk (Calbiochem, Darmstadt, Germany) for 18 h. R2/Fas preadipocyte cells were seeded at 1.5×10^4 cells per well in 96-well plates and incubated for 48 h with serially-diluted LTαs in the presence of 50 μg/mL cycloheximide. The cytotoxicities of LTαs against HEp-2 cells and R2/Fas preadipocyte cells were assessed by using the standard methylene blue assay method as previously described [12]. HT29.14S and MCF-7 cells were seeded at 5×10^3 cells per well and incubated with LTαs in the presence of 80 U/mL human Interferon γ (IFNγ) (R&D Systems) for 72 h. After incubation, cell viability was measured by using a WST-8 assay kit (Nacalai Tesque, Kyoto, Japan) according to the manufacturer's instructions. The ratio of TNFR1-/TNFR2-mediated bioactivity was calculated as follows: activity of LTαs in HEp-2 cells/activity of LTαs in R2/Fas preadipocyte cells. The TNFR1/TNFR2 ratio for wtLTα was set equal to 1.

2.6. Analysis of binding kinetics by surface plasmon resonance

The binding kinetics of LTαs were analyzed and compared by using a surface plasmon resonance (SPR) method (BIAcore 2000, GE Healthcare, UK). Human TNFR1, TNFR2, or HVEM Fc chimera (R&D Systems, Inc.) was diluted to 50 μg/mL in 10 mM sodium acetate (pH 4.5) and immobilized onto a CM5 sensor chip by using an amine coupling kit (GE Healthcare, UK) as described previously [12]. During the association phase, wtLTα or LTα mutants diluted in HBS-EP running buffer (GE, Healthcare UK) to 37, 18.5, 9.3, 4.6, or 2.3 nM were passed over the immobilized TNFRs for 2 min at a flow rate 20 μL/min. During the dissociation phase, HBS-EP was run over the sensor chip for 1 min at a flow rate 20 μ L/min. Complexes were eluted by using 20 μL of 10 mM glycine–HCl (pH 2.0). Data were evaluated by using BIAevaluation 4.1 software (GE Healthcare UK) to apply a 1:1 Langmuir binding model. The obtained sensorgrams were fitted globally over the range of injected concentrations and simultaneously over the association and dissociation phases.

2.7. Evaluation of caspase-3/7 and -8 activities

HEp-2 cells were seeded at 4×10^4 cells per well in 96-well plates and then incubated for 6, 12, or 18 h with 10 ng/mL of the relevant LTα in the presence of 50 μg/mL cycloheximide. Activities of intracellular caspase-8 and caspase-3/7 were measured by using Caspase-Glo assays (Promega, Madison, WI) according to the manufacturer's instructions.

2.8. Evaluation of NFκB activities

HEp-2 cells were co-transfected with pGL4.32, a NFκB-responsive firefly luciferase expression vector, and pRL-TK, a thymidine kinase–regulated renilla luciferase expression vector (Promega) at a ratio of 90:1 for 18 h. The cells were then treated with 10 ng/mL of wtLTα or LTα mutants for 1, 2, 4, 6, 12, and 24 h. Expression levels of intracellular firefly luciferase and renilla luciferase were then measured by using the Dual-Luciferase Reporter Assay System (Promega). The expression level of firefly luciferase was normalized against that of renilla luciferase.

3. Results

3.1. Production of a highly bioactive LTα mutant

Our recent study showed that site-specific PEGylation of a lysine-deficient mutant of LTα might be useful for cancer therapy, because the mutant retained bioactivity after PEGylation [9]. Here, we attempted to create a lysine-deficient mutant of LTα with augmented bioactivity *via* TNFR1 and TNFR1-selective bioactivity that could be used for site-specific PEGylation in the future. A phage library displaying LTα mutants with randomized sequences in place of all lysine codons was prepared. For the construction of the phage library, two-step PCR was used to replace the lysine codons randomly with an NNS sequence. As a result, we successfully constructed a library with 2×10^6 independent clones, and performed two rounds of panning against immobilized human TNFR1; phage clones were screened for binding affinity to TNFR1 by conducting an ELISA (data not shown). We obtained three LTα mutants (mutLT1, mutLT2, and mutLT3), which were putative lysine-deficient mutants of LTα. DNA sequencing analysis of the LTα mutants confirmed that all 6 lysine residues present in wtLTα were mutated to other amino acids (Table 1). To investigate the properties of the LTα mutants in detail, we prepared recombinant LTα mutant proteins by using an *E. coli* expression system, as previously described [12]. LTα mutants and wtLTα were expressed in *E. coli* and obtained through refolding of inclusion bodies. Purified LTα mutants displayed a molecular mass of 18 kDa by SDS–PAGE analysis (Fig. 1A), and a molecular mass of approximately 60 kDa by size exclusion chromatography (Fig. 1B), indicating that LTα mutants form homotrimeric complexes, as does wtLTα. The isoelectric points (pI) of mutLT1, mutLT2, and mutLT3 were 6.16, 6.16, and 6.00, respectively whereas that of wtLTα was 8.94 (Table 1). We also visually assessed the changes in the surface electrostatic potential values by using GRASP software (Fig. 1C). Because of their lack of lysine residues, LTα mutants had more negative areas on their surface than did wtLTα.

3.2. Bioactivities of LTα mutants

To assess the TNFR1-mediated bioactivity of LTα mutants, cytotoxicity assays using HEp-2 cells were performed (Fig. 2A). wtLTα and LTα mutants showed dose-dependent cytotoxicity, and the bioactivity of each LTα mutant was higher than that of wtLTα in the HEp-2 cells (Fig. 2A). The bioactivity of mutLT1 was especially high (31.8 times that of wtLTα; Table 2). Furthermore, we confirmed that the LTα-induced cytotoxicity was blocked by the anti-TNFR1 antibody in all cases (Fig. 2B). These results indicate that the LTα mutants possess higher TNFR1-mediated bioactivity than that displayed by wtLTα. To confirm that the higher bioactivity of the LTα mutants was not specific to HEp-2 cells, we examined the bio-

Table 1
Amino acid sequences and the isoelectric points of LTα mutants. The pI values of LTαs were calculated by using a program in the Expert Protein Analysis System proteomics server of the Swiss Institute of Bioinformatics (Basel, Switzerland).

	Residue position						pI
	19	28	39	84	89	119	
wtLTα	Lys	Lys	Lys	Lys	Lys	Lys	8.94
mutLT1	Asn	Gln	Asn	Ser	Leu	Gly	6.16
mutLT2	Asn	Gln	Ser	Thr	Val	Val	6.16
mutLT3	Asp	Gln	Ala	Thr	Thr	Ala	6.00

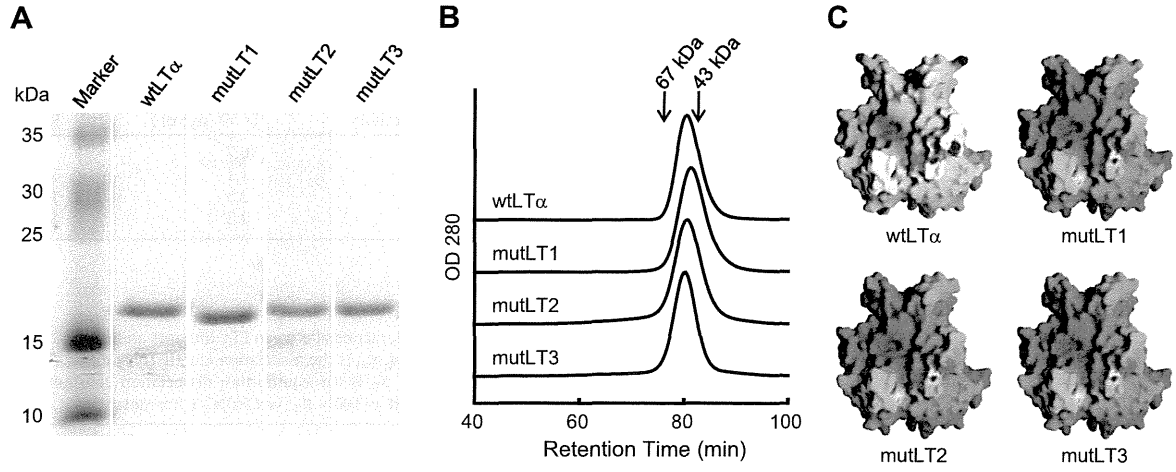

Fig. 1. Properties of recombinant LTα mutants. (A) SDS–PAGE analysis of wtLTα and LTα mutants. All products were separated on an SDS–PAGE gel and visualized by means of Coomassie Brilliant Blue staining. Marker indicates molecular weight standards. (B) Chromatograms of purified wtLTα and LTα mutants. wtLTα or LTα mutants were loaded onto a size-exclusion column and eluted at 1.0 mL/min. (C) The electrostatic potential surface was generated by using GRASP software. Red and blue indicate negative and positive electrostatic potentials, respectively. The electrostatic potential ranged from −7.5 kT (bright blue) to 7.5 kT (bright red). The relative accessible surface areas were calculated by using JOY software.

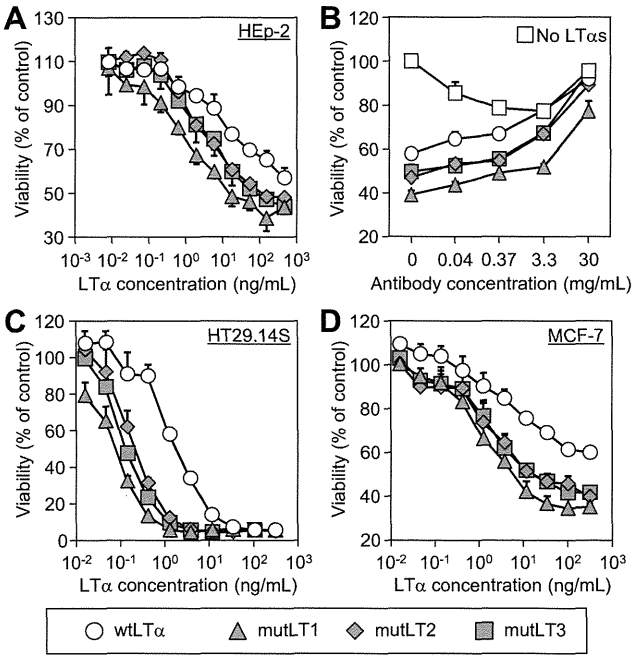

Fig. 2. TNFR1-mediated cytotoxic activity of wtLTα and LTα mutants. (A) HEp-2 cells were incubated with wtLTα or LTα mutants in the presence of cycloheximide. After 18 h incubation, cell viability was assessed by methylene blue assay. (B) HEp-2 cells were treated with serially-diluted MAB225, an anti-TNFR1 neutralizing antibody, for 30 min. The cells were then incubated with 100 ng/mL wtLTα or LTα mutants in the presence of cycloheximide. After 18 h incubation, the cell viability was assessed by methylene blue assay. (C) HT29.14S cells and (D) MCF-7 cells were incubated with wtLTα or LTα mutants in the presence of IFNγ. After 72 h incubation, the cell viability was assessed by WST-8 assay. EC30 and EC50 are the concentrations of LTα required for 30% and 50% inhibition of cell viability, respectively. Each value represents the mean ± SD ($n = 4$).

activities of mutLTαs in two other cell types (Fig. 2C and D, Table 2). When compared with wtLTα, the LTα mutants exhibited 8–24 times the cytotoxicity in HT29.14S cells, and 16–34 times the cytotoxicity in MCF-7 cells (Fig. 2C and D, Table 2). To specifically evaluate the TNFR2-mediated bioactivity of the LTα mutants, we examined the levels of cytotoxity induced by LTα mutants in hTNFR2/mFas-PA cells. These cells have been engineered to exhibit hTNFR2- but not hTNFR1-mediated activities [14]. The human TNFR2-mediated bioactivities of LTα mutants were 2.2–4.1 times those of wtLTα in hTNFR2/mFas-PA cells (Fig. 3). The calculated ratios of TNFR1-mediated bioactivity by using HEp-2 cells/TNFR2-mediated bioactivity induced by mutLT1, mutLT2, and mutLT3 were 7.8, 3.2, and 1.9 times that of wtLTα, respectively. This result suggests that LTα mutants, especially mutLT1, have selectivity for TNFR1 in addition to their augmented bioactivity.

Next, to measure the binding affinity of LTα mutants to TNFRs, we performed an SPR analysis by using a BIAcore 2000 biosensor (Table 3). The binding affinities of mutLT1, mutLT2 and mutLT3 to TNFR1 were 2.7, 2.0, and 1.4 times those of wtLTα, respectively. We considered that the increased affinity of LTα mutant for TNFR1 might be related to the enhanced bioactivity through this receptor. In particular, k_{off} values for LTα mutants binding to TNFR1 were 39–57% of the value for wtLTα, whereas the k_{on} values for LTα mutants binding to TNFR1 were almost the same as that for wtLTα. These results suggest that TNFR1 interacts more strongly with the LTα mutants than wtLTα due to slow dissociation kinetics, and that this binding mode between LTα mutant and TNFR1 induces a potent signaling pathway. We then evaluated the affinity of the LTα mutants for TNFR2 by using SPR methodology (Table 4). The affinity of TNFR2 for LTα mutants was 1.5–2.1 times that for wtLTα due to fast association kinetics. Taken together, these results indicate that the binding modes of LTα mutants to TNFR1 and TNFR2 might dictate their bioactivity.

We previously demonstrated that Lys84 in LTα plays a crucial role in the protein's interaction with the main chain of TNFR1 [12]. Therefore, to investigate the importance of the amino acid sequence at position 84, we created LTα mutants with Lys84 replaced by Ser84 (K84S), Thr84 (K84T), or Ala84 (K84A), and evaluated their binding kinetics and bioactivities *via* TNFR1. We found that these point mutants exhibited a slower dissociation rate and increased bioactivity *via* TNFR1 when compared with wtLTα. K84S showed especially high bioactivity even though its affinity for TNFR1 was lower than that of wtLTα (Table 5).

3.3. Activation of caspases by LTα mutant

It is known that TNFR1-mediated cell death is regulated by the activities of caspases including caspase-3, -7, and -8 [17].

Table 2
The TNFR1-mediated bioactivities of wtLTα and LTα mutants. EC30 and EC50 were calculated from the cytotoxic activity of wtLTα and LTα mutants against HEp-2, HT29.14S and MCF-7 cells. Relative activity values were calculated as EC30 (wtLTα)/EC30 (LTα mutant) or EC50 (wtLTα)/EC50 (LTα mutant).

	HEp-2 cells		HT29.14S cells		MCF-7 cells	
	EC30 (ng/mL)	Relative activity	EC50 (ng/mL)	Relative activity	EC50 (ng/mL)	Relative activity
wtLTα	47.7	1.0	1.80	1.0	36.7	1.0
mutLT1	1.5	31.8	0.08	23.6	1.1	33.7
mutLT2	6.8	7.0	0.21	8.5	2.3	16.0
mutLT3	7.8	6.1	0.13	14.2	2.3	16.0

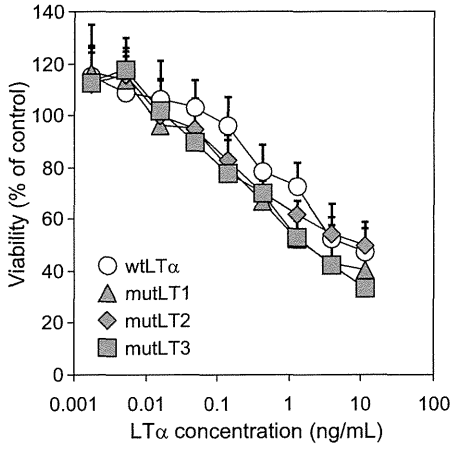

	EC30 (ng/mL)	Relative activity (% vs wtLTα)
wtLTα	1.39	100
mutLT1	0.34	409
mutLT2	0.64	217
mutLT3	0.43	323

Fig. 3. TNFR2-mediated cytotoxic activities of wtLTα and LTα mutants. hTNFR2/mFas-PA cells were incubated with serial dilutions of wtLTα or LTα mutants in the presence of cycloheximide. After 48 h incubation, cell viability was assessed by methylene blue assay. EC30 is the concentration of LTα required for 30% inhibition of cell viability. Each value represents the mean ± SD ($n = 4$).

Table 3
The binding kinetics of interactions between LTα mutants and hTNFR1 analyzed by using an SPR biosensor. k_{on} is the association kinetic constant; k_{off} is the dissociation kinetic constant; and K_D is the equilibrium dissociation constant. Relative affinity values were calculated as 100 × K_D (wtLTα)/K_D (LTα mutant).

	k_{on} (10^6/M s)	k_{off} (10^{-4}/s)	K_D (10^{-10}/M)	Relative affinity (% vs wtLTα)
wtLTα	1.2	6.1	4.9	100
mutLT1	1.3	2.4	1.8	269
mutLT2	1.4	3.5	2.5	195
mutLT3	0.97	3.4	3.4	143

Therefore, to examine the mechanism behind the augmentation of TNFR1-mediated bioactivity, we investigated the association between caspase activity and LTα mutant-induced cell death. First, we treated cells with LTα mutants in the presence of a broad caspase inhibitor, zVAD-fmk, and analyzed the cell viability (Fig. 4A). The results showed that zVAD-fmk almost completely abrogated the cytotoxicity induced by wtLTα and LTα mutants. These results indicate that both wild-type and LTα mutant-induced cell death were dependent on the activation of caspase. We then examined the activity of caspase-3/7 (Fig. 4B) and -8 (Fig. 4C) induced by LTα mutants in HEp-2 cells. LTα mutants, especially

Table 4
Binding kinetics of interactions between LTα mutants and hTNFR2 were analyzed by using an SPR biosensor. k_{on} is the association kinetic constant; k_{off} is the dissociation kinetic constant; and K_D is the equilibrium dissociation constant. Relative affinity values were calculated as 100 × K_D (wtLTα)/K_D (LTα mutant).

	k_{on} (10^6/M s)	k_{off} (10^{-4}/s)	K_D (10^{-10}/M)	Relative affinity (% vs wtLTα)
wtLTα	2.8	23.5	8.3	100
mutLT1	4.7	25.0	5.4	154
mutLT2	6.2	24.0	3.9	213
mutLT3	4.5	25.3	5.6	148

mutLT1, which has the highest bioactivity, quickly and strongly induced the activation of caspases. These results suggest that stabilization of the LTα -TNFR1 complex by the presence of LTα mutant contributed to increased caspase activity, which in turn induced cytotoxic effects.

3.4. Activation of NFκB by LTα mutants

It is well known that TNFR1 activates NFκB signaling pathway in addition to the caspase cascade [18,19]. Therefore, to investigate whether the LTα mutants activate NFκB, we assessed the association between NFκB activity and LTα mutant-induced cell death. First, we prepared cells transfected with luciferase expressing vector activated by NFκB. Then, we treated cells with LTα mutants and analyzed the NFκB activity by measuring the expression level of luciferase (Fig. 5). Despite the higher TNFR1-mediated bioactivity of LTα mutants, we found that NFκB activity was induced to a similar extent by LTα mutants and wtLTα. This finding indicates that the LTα mutants selectively activate the caspase cascade but not NFκB activation *via* TNFR1.

4. Discussion

When constructing a LTα mutant as an anti-cancer agent, it is important that the mutant exhibits TNFR1 selectivity because of the lethal side-effects of TNFR2-mediated bioactivity. We previously created a LTα mutant (R1selLT), which had only 2.5% of the TNFR2-mediated bioactivity of wtLTα and 3.5 times of the TNFR1-mediated bioactivity of wtLTα [12]. The ratio of TNFR1/TNFR2 bioactivity of R1selLT was 145.8 times that of wtLTα. In addition to TNFR1 selectivity, augmentation of TNFR1-mediated bioactivity is also highly desirable in a therapeutic agent for cancer. Here, we created three lysine-deficient LTα mutants with greatly increased levels of TNFR1-mediated bioactivity through an altered binding mode. These mutants showed preferentially augmented bioactivity *via* TNFR1 compared with TNFR2. The TNFR1 selectivity of mutLT1, 2, and 3 was 7.8, 3.2, and 1.9 times that of wtLTα, respectively. Although the TNFR1 selectivity was lower for mutLT1 than for R1selLT, the TNFR1-mediated bioactivity of mutLT1 was 31.8 times that of wtLTα compared to 3.5 times of R1selLT. Such extreme augmentation of bioactivity is rarely reported. As

Table 5
Binding kinetics of interactions between point-mutated LTαs and hTNFR1 were analyzed by using an SPR biosensor. k_{on} is the association kinetic constant; k_{off} is the dissociation kinetic constant; and K_D is the equilibrium dissociation constant. Relative affinity values were calculated as 100 × K_D (wtLTα)/K_D (point mutated LTα). TNFR1-mediated relative activities of LTα mutants were calculated from the concentration of LTα required for 30% inhibition of HEp-2 cell viability.

	k_{on} (10^6/M s)	k_{off} (10^{-4}/s)	K_D (10^{-10}/M)	Relative affinity (% vs wtLTα)	Relative activity(% vs wtLTα)
wtLTα	1.2	6.1	4.9	100	100
K84S	0.28	2.2	8.0	62	4810
K84T	1.0	4.3	118	195	1100
K84A	1.5	5.3	3.5	143	910

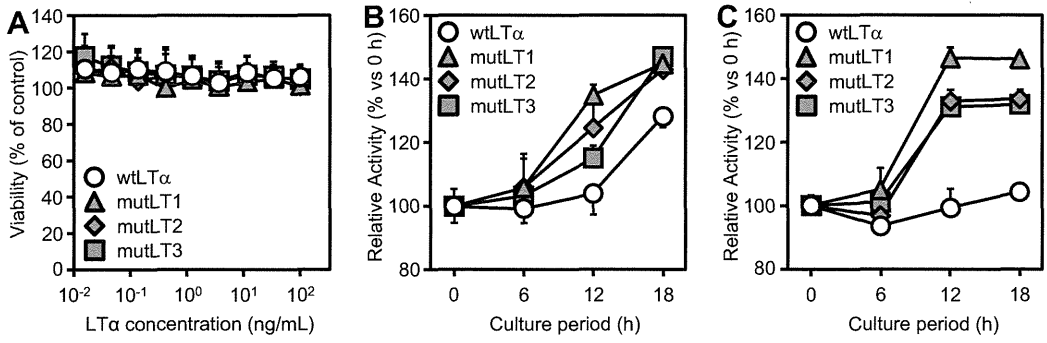

Fig. 4. Caspase activities in HEp-2 cells treated with wtLTα or LTα mutants. (A) Cycloheximide treated HEp-2 cells were incubated with wtLTα or LTα mutants in the presence of zVAD-fmk. After 18 h incubation, cell viability was assessed by methylene blue assay. (B and C) Cycloheximide treated HEp-2 cells were incubated for 6, 12, or 18 h with 10 ng/mL LTαs, and the activities of intracellular caspase-3/7 (B) and intracellular caspase-8 (C) were measured by using Caspase-Glo assays. Each value represents the mean ± SD (n = 4).

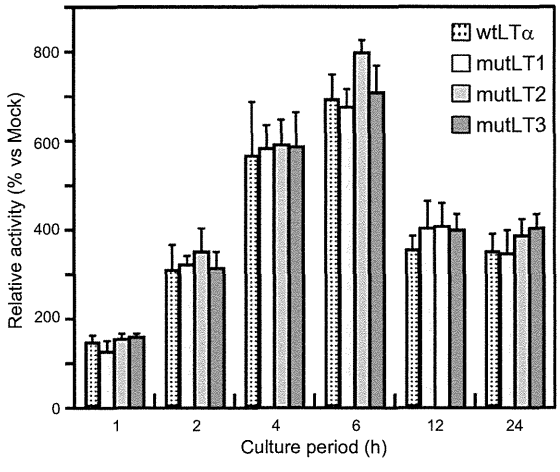

Fig. 5. NFκB activities in HEp-2 cells treated with wtLTα or LTα mutants. HEp-2 cells were co-transfected with pGL4.32 and pRL-TK (Promega). Eighteen hours after transfection, the cells were treated with 10 ng/mL LTαs for the indicated period. The intracellular luciferase activity was then quantified. Data are shown as the relative NFκB activity compared with the mock-transfected group. Each bar represents the mean ± SD (n = 4).

described above, high TNFR1 selectivity of R1selLT was mainly resulted from the significant decreased TNFR2-mediated bioactivity. On the other hand, the TNFR1 selectivity of mutLT1 was obtained from the augmented TNFR1-mediated bioactivity, while TNFR2-mediated bioactivity was maintained. On this point, TNFR2 is known to play essential role for the induction of immune responses. Therefore, we consider that a TNFR1-selective LTα mutants with high TNFR1-mediated and equivalent TNFR2-mediated bioactivity compared to wtLTα, such as mutLT1, would be a superior candidate for cancer therapy by combination of direct pro-apoptotic effects of LTα on tumor cells and an enhancement of local/systemic immunity.

Many cellular signaling processes are hypothesized to depend not only on the equilibrium strength of the ligand–receptor interactions but also on the average durations or kinetic dissociation rates of these interactions [20–23]. In some cases, the intensity of distal signaling depends on the off-rate rather than on the on-rate of the ligand–receptor complex [20,22]. For interactions with TNFR1, the LTα mutants exhibited higher k_{off} values compared with the value for wtLTα, whereas the k_{on} values for the LTα mutants were almost same as that for wtLTα. In addition, the bioactivity of wtLTα and LTα mutants was related to k_{off} but not to k_{on}. These data suggest that the LTα mutants interact with TNFR1 by slow dissociation and induce robust signal transduction. In contrast, for interactions with TNFR2, the LTα mutants showed a higher k_{on} than that for wtLTα, whereas the k_{off} values for the LTα mutants was almost same as that for wtLTα. These data indicate that the detailed molecular dissection of ligand-receptor binding kinetics is important for the construction of functional LTα mutants with desired TNFR-mediated bioactivity.

We previously demonstrated that Lys84 of LTα plays a crucial role in the protein's interaction with the main chain of TNFR1 [12]. Here, to explore the role of Lys84 further, we created LTα mutants with Lys84 replaced by Ser84 or Thr84, and found that the mutant with Ser84 showed slower dissociation kinetics and increased bioactivity when compared with wtLTα or the other mutants (Table 5). These results suggest that Lys84 contributes to the TNFR1-mediated bioactivity and the binding kinetics of the TNFR1–LTα interaction. In all three mutants analyzed here, the amino acid Lys at position 28 was changed to Gln (Table 1). Whereas these mutants exhibited increased TNFR1-mediated bioactivity, our previous data showed that a mutant with a K28Q substitution had decreased TNFR1-mediated bioactivity compared with that of wtLTα. Furthermore, mutLT2, which has the Lys at position 39 replaced by Ser, showed slightly increased TNFR2-mediated bioactivity, but a mutant containing the equivalent substitution at the same position showed decreased TNFR2-mediated bioactivity in our previous study [12]. These results suggest

that the sum of the mutations, including those at positions 28 and 39, were responsible for the augmented binding affinities to TNFR1 and TNFR2.

TNFR1 triggers apoptotic caspase signaling following activation of Fas-associated protein with death domain (FADD) [17]. At the same time, triggering of TNFR1 signals induces the anti-apoptotic NFκB cascade following the activation of TNF receptor-associated death domain (TRADD) and TNF receptor-associated factor (TRAF) adaptors [18,19,24]. Active NFκB induces transcription of a set of genes encoding anti-apoptotic proteins [25,26]. Therefore, in many cell types, TNF α has no apoptotic effects due to the parallel triggering by TNF α of a signaling pathway that activates NFκB *via* the TRADD and TRAF adaptors. Here, however, we found that the LTα mutants, which showed augmented bioactivity *via* TNFR1, efficiently induced caspase activation but induced NFκB to the same level as that induced by wtLTα (Figs. 4 and 5). We consider that the slower rate of dissociation of the LTα mutants from TNFR1 was important to the activation of FADD signaling cascade, but not to the activation of TRADD and TRAF adaptors. We speculate that the alteration of the binding mode of LTα mutant to TNFR1 increased the caspase signaling pathway, but not TRADD- and TRAF-mediated NFκB signaling. These findings will facilitate the construction of functional LTα mutants with even higher receptor selectivity and bioactivity in the future.

5. Conclusions

Here, we created highly bioactive LTα mutants with TNFR1-selectivity by using a phage display technique, and we clarified the molecular basis of their augmented TNFR1-mediated bioactivity. A better understanding of the correlation between structure, kinetic behavior, and activity will likely accelerate drug discovery because it will increase awareness of the properties of therapeutic proteins. We suggest that LTα mutants have the potential to be a powerful tool for cancer therapy by combination of direct pro-apoptotic effects of LTα on tumor cells and an enhancement of local/systemic immunity, and that our findings provide valuable information for the construction of even more functional LTα mutants.

Acknowledgements

The authors declare that they have no conflict of interests. This study was supported in part by grants from the Ministry of Health, Labor, and Welfare in Japan; by the Research on Health Sciences focusing on Drug Innovation from the Japan Health Sciences Foundation; and by the Takeda Science Foundation.

References

[1] Neumann B, Luz A, Pfeffer K, Holzmann B. Defective Peyer's patch organogenesis in mice lacking the 55-kD receptor for tumor necrosis factor. J Exp Med 1996;184:259–64.
[2] Kratz A, Campos-Neto A, Hanson MS, Ruddle NH. Chronic inflammation caused by lymphotoxin is lymphoid neogenesis. J Exp Med 1996;183:1461–72.
[3] Koni PA, Sacca R, Lawton P, Browning JL, Ruddle NH, Flavell RA. Distinct roles in lymphoid organogenesis for lymphotoxins alpha and beta revealed in lymphotoxin beta-deficient mice. Immunity 1997;6:491–500.
[4] Schrama D, thor Straten P, Fischer WH, McLellan AD, Brocker EB, Reisfeld RA, et al. Targeting of lymphotoxin-alpha to the tumor elicits an efficient immune response associated with induction of peripheral lymphoid-like tissue. Immunity 2001;14:111–21.
[5] Schrama D, Voigt H, Eggert AO, Xiang R, Zhou H, Schumacher TN, et al. Immunological tumor destruction in a murine melanoma model by targeted LTalpha independent of secondary lymphoid tissue. Cancer Immunol Immunother 2008;57:85–95.
[6] Ryan SM, Mantovani G, Wang X, Haddleton DM, Brayden DJ. Advances in PEGylation of important biotech molecules: delivery aspects. Expert Opin Drug Deliv 2008;5:371–83.
[7] Yamamoto Y, Tsutsumi Y, Yoshioka Y, Nishibata T, Kobayashi K, Okamoto T, et al. Site-specific PEGylation of a lysine-deficient TNF-alpha with full bioactivity. Nat Biotechnol 2003;21:546–52.
[8] Shibata H, Yoshioka Y, Ikemizu S, Kobayashi K, Yamamoto Y, Mukai Y, et al. Functionalization of tumor necrosis factor-alpha using phage display technique and PEGylation improves its antitumor therapeutic window. Clin Cancer Res 2004;10:8293–300.
[9] Narimatsu S, Yoshioka Y, Watanabe H, Masano T, Morishige T, Yao X, et al. Lysine-deficient lymphotoxin-alpha mutant for site-specific PEGylation. Cytokine 2011;56:489–93.
[10] Everaerdt B, Brouckaert P, Shaw A, Fiers W. Four different interleukin-1 species sensitize to the lethal action of tumour necrosis factor. Biochem Biophys Res Commun 1989;163:378–85.
[11] Brouckaert P, Libert C, Everaerdt B, Fiers W. Selective species specificity of tumor necrosis factor for toxicity in the mouse. Lymphokine Cytokine Res 1992;11:193–6.
[12] Yoshioka Y, Watanabe H, Morishige T, Yao X, Ikemizu S, Nagao C, et al. Creation of lysine-deficient mutant lymphotoxin-alpha with receptor selectivity by using a phage display system. Biomaterials 2010;31:1935–43.
[13] Browning JL, Miatkowski K, Sizing I, Griffiths D, Zafari M, Benjamin CD, et al. Signaling through the lymphotoxin beta receptor induces the death of some adenocarcinoma tumor lines. J Exp Med 1996;183:867–78.
[14] Abe Y, Yoshikawa T, Kamada H, Shibata H, Nomura T, Minowa K, et al. Simple and highly sensitive assay system for TNFR2-mediated soluble- and transmembrane-TNF activity. J Immunol Methods 2008;335:71–8.
[15] Nicholls A, Sharp KA, Honig B. Protein folding and association: insights from the interfacial and thermodynamic properties of hydrocarbons. Proteins 1991;11:281–96.
[16] Mizuguchi K, Deane CM, Blundell TL, Johnson MS, Overington JP. JOY: protein sequence-structure representation and analysis. Bioinformatics 1998;14:617–23.
[17] Sheikh MS, Huang Y. Death receptor activation complexes: it takes two to activate TNF receptor 1. Cell Cycle 2003;2:550–2.
[18] Chen G, Goeddel DV. TNF-R1 signaling: a beautiful pathway. Science 2002;296:1634–5.
[19] Magne N, Toillon RA, Bottero V, Didelot C, Houtte PV, Gerard JP, et al. NF-kappaB modulation and ionizing radiation: mechanisms and future directions for cancer treatment. Cancer Lett 2006;231:158–68.
[20] Hlavacek WS, Redondo A, Metzger H, Wofsy C, Goldstein B. Kinetic proofreading models for cell signaling predict ways to escape kinetic proofreading. Proc Nat Acad Sci USA 2001;98:7295–300.
[21] Liu ZJ, Haleem-Smith H, Chen H, Metzger H. Unexpected signals in a system subject to kinetic proofreading. Proc Nat Acad Sci USA 2001;98:7289–94.
[22] Krippner-Heidenreich A, Tubing F, Bryde S, Willi S, Zimmermann G, Scheurich P. Control of receptor-induced signaling complex formation by the kinetics of ligand/receptor interaction. J Biol Chem 2002;277:44155–63.
[23] Torigoe C, Faeder JR, Oliver JM, Goldstein B. Kinetic proofreading of ligand–FcepsilonRI interactions may persist beyond LAT phosphorylation. J Immunol 2007;178:3530–5.
[24] Kim JY, Lee JY, Kim DG, Koo GB, Yu JW, Kim YS. TRADD is critical for resistance to TRAIL-induced cell death through NF-kappaB activation. FEBS Lett 2011;585:2144–50.
[25] Arch RH, Gedrich RW, Thompson CB. Tumor necrosis factor receptor-associated factors (TRAFs) – a family of adapter proteins that regulates life and death. Genes Dev 1998;12:2821–30.
[26] Deveraux QL, Reed JC. IAP family proteins–suppressors of apoptosis. Genes Dev 1999;13:239–52.

Laboratories of Bio-Functional Molecular Chemistry[1] and Toxicology and Safety Science[2], Graduate School of Pharmaceutical Sciences, Osaka University, Japan

Hepatotoxicity of sub-nanosized platinum particles in mice

Y. YAMAGISHI[1], A. WATARI[1], Y. HAYATA[1], X. LI[1], M. KONDOH[1], Y. TSUTSUMI[2], K. YAGI[1]

Received July 19, 2012, accepted August 30, 2012

Dr. Akihiro Watari, Laboratory of Bio-Functional Molecular Chemistry, Graduate School of Pharmaceutical Sciences, Osaka University, Suita, Osaka 565-0871, Japan
akihiro@phs.osaka-u.ac.jp

Pharmazie 68: 178–182 (2013) *doi: 10.1691/ph.2013.2141*

Nano-sized materials are widely used in consumer products, medical devices and engineered pharmaceuticals. Advances in nanotechnology have resulted in materials smaller than the nanoscale, but the biologic safety of the sub-nanosized materials has not been fully assessed. In this study, we evaluated the toxic effects of sub-nanosized platinum particles (snPt) in the mouse liver. After intravenous administration of snPt (15 mg/kg body weight) into mice, histological analysis revealed acute hepatic injury, and biochemical analysis showed increased levels of serum markers of liver injury and inflammatory cytokines. In contrast, administration of nano-sized platinum particles did not produce these abnormalities. Furthermore, snPt induced cytotoxicity when directly applied to primary hepatocytes. These data suggest that snPt have the potential to induce hepatotoxicity. These findings provide useful information on the further development of sub-nanosized materials.

1. Introduction

Nanotechnology involves manipulation of matter on the scale of the nanometer and has the potential to improve quality of life via functional products. Nanomaterials are commonly defined as objects with dimensions of 1 to 100 nm and are now widely used in electronics, catalysts, clothing, drugs, diagnostic devices, and cosmetics (Baughman et al. 2002; Patra et al. 2010; Service et al. 2007; Ariga et al. 2010). Recent progress in the field has allowed the creation of sub-nanosized materials that have different physicochemical properties, including improved conductivity, durability and strength. Although these materials may be useful for industrial and scientific purposes, the biologic safety of these materials has not been fully evaluated (Nel et al. 2006; Oberdorster et al. 2005).

Nano-sized platinum particles (nPt) are used for industrial applications and in consumer products, such as cosmetics, supplements and food additives (Gehrke et al. 2011; Horie et al. 2011). The biological influence of exposure to nPt has been previously investigated. For example, nPt has anti-oxidative activity (Watanabe et al. 2009; Onizawa et al. 2009; Kajita et al. 2007), and may be useful for the medical treatment of diseases related to oxidative stress and aging. However, some reports suggest that these substances can induce inflammation in mice or impair DNA integrity (Pelka et al. 2009; Park et al. 2010). Thus, the understanding of the biological influences of nPt has still not been definitively established, and our knowledge regarding the biological effects of sub-nanosized platinum particles (snPt) is severely lacking.

Nano-sized particles can enter and penetrate the lungs, intestines and skin. The degree of penetration depends on the size and surface features of the nano-sized particle. Furthermore, nanoparticles can enter the circulatory system and migrate to various organs, such as the brain, spleen, liver, kidney and muscles (Zhu et al. 2008; Furuyama et al. 2009; Oberdorster et al. 2004; Ai et al. 2011). The liver is a vital organ that is involved in the uptake of nutrients and the elimination of waste products and pathogens from the blood; it is also an important organ for the clearance of nanoparticles. However, some nanoparticles are hepatotoxic (Nishimori et al. 2009a, b; Ji et al. 2009; Cho et al. 2009; Folkmann et al. 2009). In the present study, we investigated the influence of sub-nanosized platinum particles (snPt) on the liver.

2. Investigations and results

To investigate the acute liver toxicity of snPt, we administered snPt (15 mg/kg body weight) into mice by intravenous injection. Histological analysis revealed acute hepatic injury, including vacuole degeneration (Fig. 1). Furthermore, administration of snPt at doses over 15 mg/kg resulted in significant elevation of serum alanine aminotransferase (ALT) and aspartate aminotransferase (AST) levels (Fig. 2A and B) and of interleukin-6 (IL-6) levels (Fig. 2C). ALT and AST levels were increased at 3 h to 24 h after intravenous administration at 20 mg/kg snPt (Fig. 3A and B). Cell viability assessment by WST assay demonstrated that direct treatment of isolated hepatocytes with snPt at concentrations of 0.1, 1, 10, 50 and 100 μg/ml resulted in a dose-dependent decrease in hepatocyte viability when compared with vehicle-treated cells (Fig. 4). These observations suggest that snPt induced inflammation and hepatocyte death.

Previous reports showed that biological influences of nanomaterials vary according to material size (Nishimori et al. 2009a, b; Jiang et al. 2008; Oberdorster et al. 2010). Therefore, we examined whether nPt, with a diameter of approximately 15 nm, leads

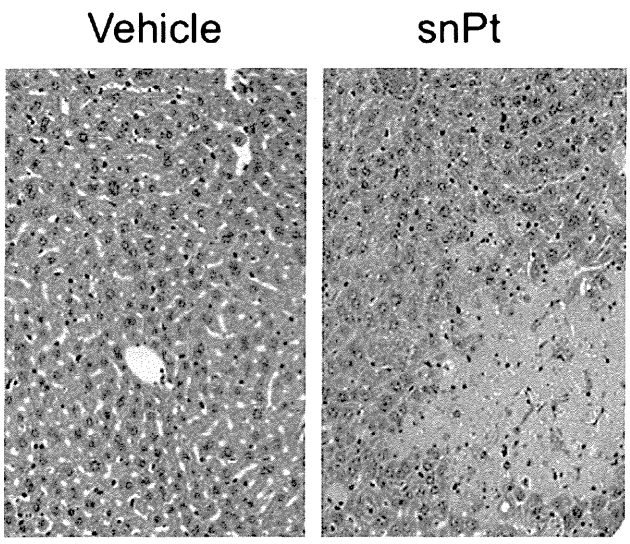

Fig. 1: Histological analysis of liver tissues in snPt-treated mice. snPt was intravenously administered to mice at 15 mg/kg. At 24 h after administration, livers were collected and fixed with 4% paraformaldehyde. Tissue sections were stained with hematoxylin and eosin and observed under a microscope. The pictures show representative data from at least four mice

to a different biologic effect than snPt. As shown in Fig. 5, snPt administration resulted in dose-dependent increases in serum ALT and AST levels, whereas nPt did not. Furthermore, IL-6 levels did not change in response to administration of nPt. These results suggest that the biological effects of platinum particles are dependent on their size.

3. Discussion

The influence of size and of physiochemical properties of nanoparticles on their biologic safety is an important issue. Animal experiments have demonstrated rapid translocation of nanoparticles from the entry site to various organs (Almeida et al. 2011). In particular, nanoparticles tend to concentrate in the liver and are cleared from the body in the feces and urine after intravenous infusion (Ai et al. 2011). While the liver plays a pivotal role in the clearance of nanoparticles, some nanomaterials can induce liver injury. Therefore, we assessed the influence of snPt on the liver and demonstrated that snPt induced liver toxicity *in vitro* and *in vivo*.

Some studies have reported that nPt exert anti-oxidant and anti-inflammatory effects (Watanabe et al. 2009; Onizawa et al. 2009; Kajita et al. 2007), while other studies reported that nPt have negative biological effects. For example, treatment of a human colon carcinoma cell line with nPt resulted in a decrease in cellular glutathione level and impairment in DNA integrity (Pelka et al. 2009). Furthermore, Park et al. (2010) found that nPt prepared from K_2PtCl_6 may induce an inflammatory response in mice. In this study, we found that snPt damaged liver tissues and induced inflammatory cytokines. Kupffer cells present in liver sinusoids may mediate this process via phagocytosis of the particles and subsequent release of inflammatory cytokines. However, when we added snPt to primary hepatocytes, the viability of the cells was significantly reduced, suggesting that snPt may also exert a direct hepatotoxic effect. Thus, the cellular influences of Pt nano- and sub-nano particles may be dependent on the target cells as well as on the size and physical and chemical properties of the particles.

snPt may damage other tissues as well. Cisplatin, a first-line chemotherapy for most cancers, is a platinating agent that can cause kidney damage (Daugaard et al. 1990; Brabec et al. 2005). Furthermore, snPt-induced increases in systemic IL-6 may cause damage to various organs. Further analysis of the distribution and toxic effects of snPt is necessary.

Widespread application of sub-nanosized materials comes with an increased risk of human exposure and environmental release, and the future of nanotechnology will depend on the public acceptance of the risk-benefit ratio. The present study demonstrated that snPt induces hepatotoxicity *in vitro* and *in vivo*. However, our research also indicates that the toxicity of platinum particles could be reduced by altering their size. Additionally, biocompatible coatings can reduce the negative effects of nanoparticles on cells (Oberdorster et al. 2010; Nabeshi et al. 2011; Singh et al. 2007; Clift et al. 2008). Therefore, future studies will contribute to the development of sub-nanosized materials and will also help produce safer products.

4. Experimental

4.1. Materials

Platinum particles with a diameter of 15 nm (nPt) and less than 1 nm (snPt) were purchased from Polytech & Net GmbH (Rostock, Germany). The

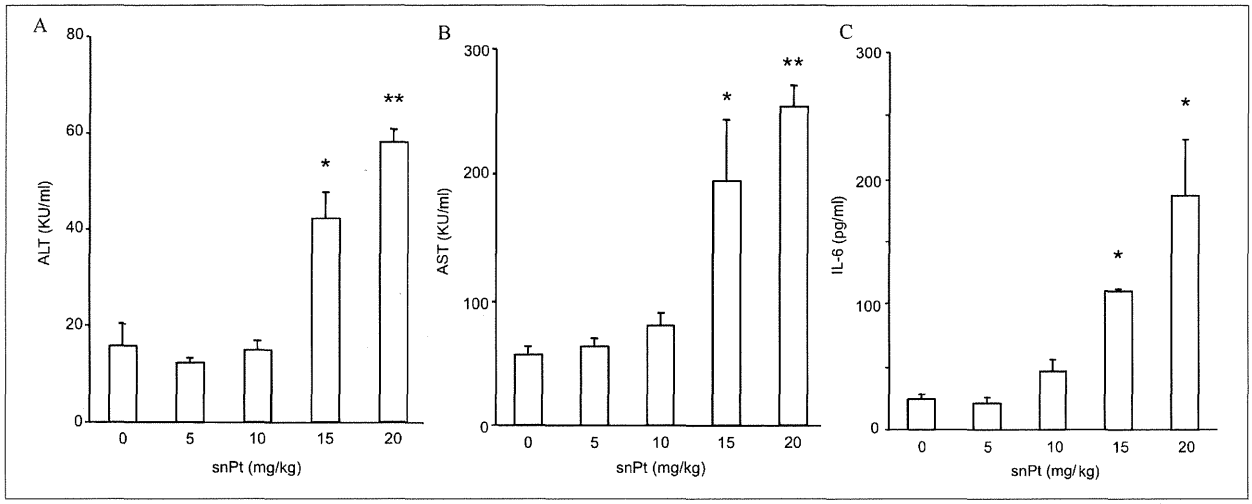

Fig. 2: Dose dependency of snPt-induced liver injury. snPt was intravenously administrated at 5, 10, 15 and 20 mg/kg. At 24 h after administration, blood was recovered, and the resultant serum was used for measurement of ALT (A), AST (B) and IL-6 (C), as described in the "Experimental" section. Data are means ± SEM (n = 3). *Significant difference when compared with the vehicle-treated group (*, $p < 0.05$, **, $p < 0.01$)

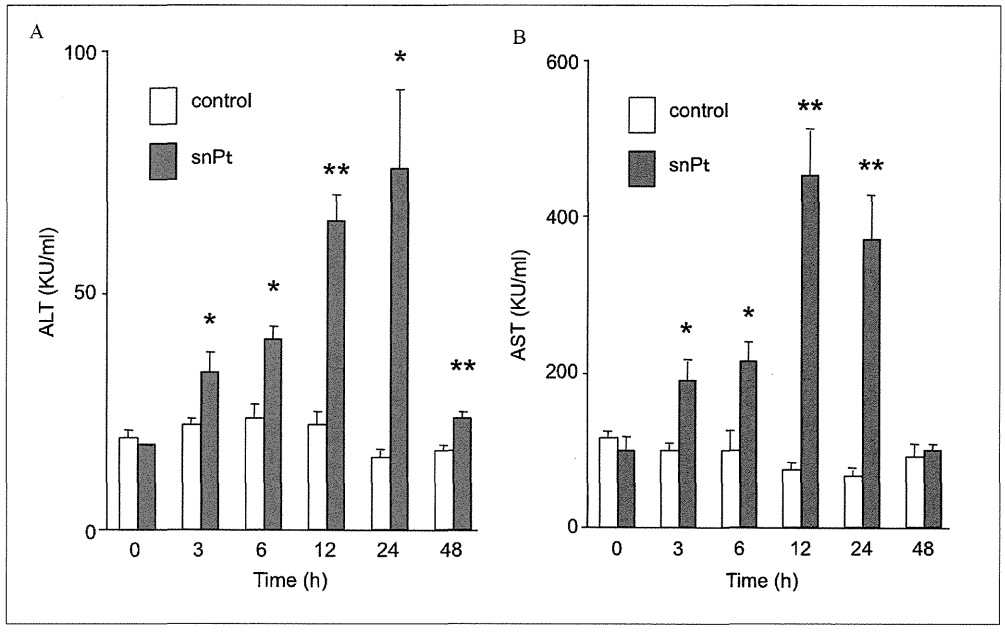

Fig. 3: Time-dependent changes of a biological marker of liver injury. snPt was intravenously administered to mice at 15 mg/kg. Blood was recovered at 3, 6, 12, 24 and 48 h after administration. The serum was used for measurement of ALT (A) and AST (B), as described in the "Experimental" section. Data are means ± SEM (n = 3). *Significant difference when compared with the vehicle-treated group (*, $p < 0.05$, **, $p < 0.01$)

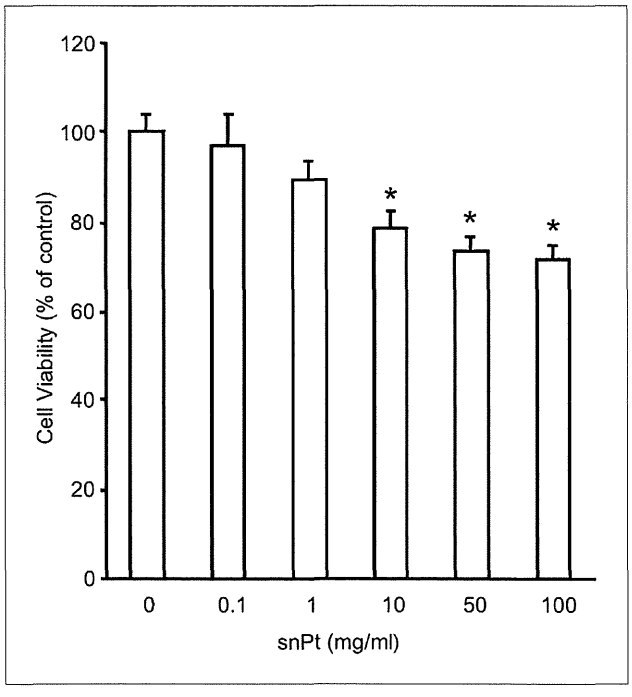

Fig. 4: Cytotoxicity of snPt in hepatic cells. Primary hepatocytes were treated with snPt at 0.1, 1, 10, 50 or 100 μg/ml. After 24 h of culture, cell viability was evaluated with the WST assay, as described in the "Experimental" section. Data are means ± SEM (n = 3). *Significant difference when compared with the vehicle-treated group ($P < 0.05$)

particles were stocked in a 5 mg/ml aqueous suspension. The stock solutions were suspended using a vortex mixer before use. Reagents used in this study were of research grade.

4.2. Animals

BALB/c male mice (8 weeks old) were obtained from Shimizu Laboratory Supplies Co., Ltd. (Kyoto, Japan), and were housed in an environmentally controlled room at 23 ± 1.5 °C with a 12 h light/12 h dark cycle. Mice had access to water and commercial chow (Type MF, Oriental Yeast, Tokyo, Japan). Mice were intravenously injected with nPt or snPt at 5 to 20 mg/kg body weight. The experimental protocols conformed to the ethical guidelines of the Graduate School of Pharmaceutical Sciences, Osaka University.

4.3. Cells

Mouse primary hepatocytes were isolated from BALB/c mice (Shimizu Laboratory Supplies Co.) by the collagenase-perfusion method (Seglen 1976). Isolated hepatocytes were suspended in Williams' E medium containing 10% fetal calf serum, 1 nM insulin, and 1 nM dexamethasone. Next, cell viability was assessed by Trypan blue dye exclusion. Cells that were at least 90% viable were used in this study. Cells were cultured in a humidified 5% CO_2 incubator at 37 °C.

4.4. Histological analysis

After intravenous administration of snPt, mouse livers were removed and fixed with 4% paraformaldehyde. Thin tissue sections were stained with hematoxylin and eosin for histological observation.

4.5. Biochemical assay

Serum alanine aminotransferase (ALT) and aspartate aminotransferase (AST) were measured using commercially available kits (WAKO Pure Chemical, Osaka, Japan), respectively. Interleukin-6 (IL-6) levels were measured with an ELISA kit (BioSource International, Camarillo, CA, USA). These assays were performed according to the manufacturer's protocols.

4.6. Cell viability assay

Cell viability was determined using WST-8 (Nacalai Tesque, Osaka, Japan), according to the manufacturer's protocol. Briefly, 1×10^4 cells/well were seeded on a 96 well plate at 37 °C overnight. After 24 h of treatment with snPt, WST-8 reagent was added to each well. The plate was incubated for 1 h at 37 °C and assessed at an absorbance of 450 nm by a plate reader. Obtained data were normalized to the control group, which was designated as 100%.

4.7. Statistical analysis

Data are presented as means ± SD. Statistical analysis was performed by student's t-test. $P < 0.05$ was considered statistically significant.